Brilliant Cresyl Blue (BCB) enhanced optoacoustic imaging enables non-destructive imaging of mammalian ovarian follicles for artificial reproduction

Rahul Dutta[1+], Subhamoy Mandal [2,3+], Hsiao-Chun Amy Lin2[2,4], Tal Raz[1], Alexander Kind[5], Angelika Schnieke[5], and Daniel Razansky[2,6]

[1]*Koret school of veterinary Medicine, The Robert H. Smith Faculty of Agriculture, Food and Environment - Hebrew University of Jerusalem, Israel*

[2]*Institute for Biological and Medical Imaging, Helmholtz Center Munich, Neuherberg, Germany*

[3]*Department of Electrical and Computer Engineering, Technical University of Munich, Germany*

[4]*iThera Medical GmbH, Munich, Germany*

[5]*Chair of Livestock Biotechnology, Technical University of Munich, Germany*

[6]*Institute for Biomedical Engineering and Institute of Pharmacology and Toxicology, University of Zurich and ETH Zurich, Switzerland*

+ equal contribution

Abstract

In the field of reproductive biology, there is a strong need for a suitable tool capable of non-destructive evaluation of oocyte viability and function. We studied the application of brilliant cresyl blue (BCB) as an intra-vital exogenous contrast agent using multispectral optoacoustic tomography (MSOT) for visualization of porcine ovarian follicles. The technique provided excellent molecular sensitivity, enabling the selection of competent oocytes without disrupting the follicles. We further conducted in vitro embryo culture, molecular analysis (real-time and reverse transcriptase PCR) and DNA fragmentation analysis to comprehensively establish the safety of BCB-enhanced MSOT imaging in monitoring oocyte viability. Overall, the experimental results suggest that the method offers a significant advance in the use of contrast agents and molecular imaging for reproductive studies. Our technique improves the accurate prediction of ovarian reserve significantly and, once standardized for in vivo imaging, could provide an effective tool for clinical infertility treatment.

**Communications are to be directed to: s.mandal@tum.de; rahul.dutta@mail.huji.ac.il; danir@ethz.ch;*

Introduction

The term "ovarian reserve" describes a woman's reproductive potential, specifically the number and quality of oocytes her ovaries contain [1]. Ovarian reserve is a complex clinical phenomenon influenced by multiple factors like age, genetics, and environmental variables [2]. Female ovaries undergo irreversible decline of the reserve starting from birth, eventually ending in menopause at a later age. Accurately predicting the rate of decline remains a challenging question to the researchers and clinicians. The tests for ovarian reserve include both biochemical tests like Follicle Stimulating Hormone (FSH) and Anti-Müllerian Hormone (AMH) detection and ultrasound imaging of the ovaries. Commonly used biochemical assays serve as a proxy for oocyte quantity but are considered poor predictors of oocyte quality [1]. Thus, medical imaging technologies have slowly emerged as an indispensable component of artificial reproductive technology (ART) for the treatment of infertility [3]. Existing diagnostic imaging technologies, such as pelvic magnetic resonance imaging (MRI) and ultrasonic imaging (US), have provided valuable insights into the mammalian reproductive system. However, the imaging contrast and spatial resolution of these methods are far inferior to those routinely obtained with optical microscopy. Ultrasonographic follicular imaging, the primary tool for oocyte retrieval *in vitro* fertilization (IVF) and embryo culture, reveals the growing follicle only as a black bubble [4]. Folliculometric information, such as follicular wall thickness, is determined by manual or semi-automated segmentation and provides only crude information with questionable predictive value[5]. Determination of oocyte quality is vital in assisted reproduction, but there has not yet been any assessment method that does not disrupt the follicle structure. Researchers and clinical practitioners are in urgent need of an innovative imaging method that reliably predicts oocyte viability and developmental competence. A non-destructive method that reliably predicts the

developmental competence of an oocyte inside an ovarian follicle would be of great benefit to IVF studies. The ability to assess the quality of the ovarian reserve pool non-invasively can have a revolutionizing effect on female reproductive health management.

The study aims to establish brilliant cresyl blue (BCB)[6] as a contrast agent for non-destructive evaluation of oocyte quality. But contrast enhancement for imaging interventions using BCB has not so far been attempted in ovarian follicle imaging. A favorable toxicity profile, relative ease of use, and inexpensive nature makes BCB an ideal candidate for a contrast agent.

BCB has previously been used effectively to identify developmentally competent oocytes without compromising oocyte viability[7]·[8]·[9]·[10]. BCB is reduced by the intracellular activity of glucose-6-phosphate dehydrogenase (G6PDH), a pentose phosphate pathway enzyme, the activity of which gradually decreases as oocytes reach the growth phase[11]. Oocytes in the mature growth phase do not reduce BCB and exhibit a blue-colored cytoplasm (BCB+ve). Growing oocytes have a high level of G6PDH activity, resulting in a colorless oocyte cytoplasm (BCB−ve)[12]. MSOT was employed as molecular imaging method capable of selectively quantifying the distribution of specific biomarkers using multiple excitation wavelengths and delivers optical contrast at unprecedented resolution and penetration depths [13][14]. The method has previously been applied to image fluorescent proteins in model organisms [15], and for tracking perfusion profiles of contrast agents and blood oxygenation *in vivo* [16]. MSOT utilizes non-ionizing radiation (near-infrared range) with safe levels of optical flux (< 15mJ/pulse on the surface of the imaged tissue), making it attractive for non-destructive cellular imaging. However, the use of optoacoustic for imaging reproductive cell has been limited. Viator et al has used photoacoustic flowmetry to detect sperm samples in a dilute solution [17], and Wittmann et al. has employed MSOT to study blood-testis barrier. To the best of our knowledge, the current study

provides the first experimental results of non-destructively imaging viable oocytes from mammalian sources.

We conducted the imaging trials *in vitro* by injecting BCB into porcine ovarian follicles and imaging the intact ovarian structure *ex vivo*. Spectral unmixing[18] and image analysis techniques[19] were used on acquired MSOT images to quantify image contrast and identify suitable follicles with competent oocytes. The MSOT results were further validated using a state-of-the-art selective plane illumination microscopy (SPIM) tool. In this way, both the anatomy and contrast agent distribution[20] were visualised, gaining precise folliculometric information, including volume, anatomical position, structural details and oocyte size. To investigate whether the procedure is toxic to the oocytes in any way, oocytes from the tested follicles were isolated and cultured *in vitro* then analyzed by real-time and reverse transcriptase PCR and DNA fragmentation analysis.

The results conclusively prove that the administration of BCB and MSOT imaging doesn't impact the viability of reproductive units, i.e., oocytes. Our experimentations support the usefulness of BCB enhanced MSOT imaging as simple, gentle and efficient translational imaging method of monitoring oocyte viability. Thus, the current study opens up new possibilities for workflow optimization and risk-mitigation in ART.

Experimental methods and results

Spectral evaluation of BCB and experimental protocol for imaging of follicles

A commercial MSOT system (inVision 256TF, iThera Medical GmbH, Munich, Germany) was used to probe a narrow window of BCB contrast in the near-infrared range (wavelengths 680-900nm). Given the inherent noise and low-contrast in ex-vivo imaging samples, we employed

non-negative constrained modelbased image reconstruction [21,22] and automatic calibration methods [23] to improve image quality. Recent studies have shown that optoacoustic spectrum is often not correlated the absorption spectrum of chromophores. Additionally, Luke et al has shown that ≥ 5 wavelengths are required to have a stable concentration estimate of a chromophore during spectroscopic optoacoustic imaging [24]. As described previous in [25], we diluted a 13mM stock solutions of 1M BCB in Dulbecco's phosphate-buffered saline (DPBS) to a 6 working concentration (25x to 250x dilutions). We used 10 wavelengths derived the reference optoacoustic spectrum for BCB at the designated concentrations [26]. An automatic segmentation and tracking algorithm developed in-house [19] was used to automatically annotate the region of interest (ROI) (approximately 25± 2 pixels) in real-time and 50 frame averaging was done to achieve high SNR. As illustrated in figure 1, optoacoustic spectral evaluation revealed that 260μM (50 times dilution) BCB provided satisfactory signal recovery without quenching. This concentration was subsequently used throughout the experimentation and imaging trials. Figure 2 illustrates the phases in the entire ovarian imaging protocol (5 phases) standardized for the study. Ovarian follicles were first injected with BCB solution using a fine bore needle (31G). Follicles contain follicular fluid that further dilutes BCB, so injection concentrations were conservatively overestimated by 10% volume (figure 2.1). The ovaries were then placed on a polyethylene sheet supplied with DPBS solution, and placed in the imaging domain submerged in deionized water at 34°C for the MSOT imaging (figure 2.2). In figure 2.3 the single wavelength image acquired at 690 nm shows the internal anatomy of the extracted ovary after the injection of BCB. To clearly identify the locations where BCB is deposited relative to tissue morphology, we spectrally unmixed the MSOT signals into two channels (BCB and tissue). The BCB channel showed deposition along the walls of the follicles (figure 2.3- spectrally resolved image). We used five different wavelengths (680nm, 690nm, 700nm, 710nm, and 850nm) to acquire the spectral dataset.

A vertex-component analysis (VCA) based blind spectral unmixing algorithm[27] was used to isolate location of the BCB chromophores. The individual follicles were isolated and the cumulus-oocyte complexes (COCs) manually extracted and visually evaluated by optical microscopy. Figure 2.4 shows the microscopic images of COCs graded for validation of the results. We have also developed automated oocyte grading algorithms based on machine learning techniques[28,29], but full descriptions are beyond the scope of this account. In the final stage of the workflow, we attempted *in vitro* embryo culture of irradiated oocytes (figure 2.5) to ascertain viability.

In figure 3.a, we show the unmixed BCB channel and the site of extraction of the chosen oocyte (insert marked with box). However, looking at a 2D frame does not provide correct size estimate of the follicle. Thus, we included the 3D rendering of the full ovarian mass by stacking multiple scan slices along the Z-direction scanned at a distance of 0.1mm (figures. 3. b). The 3D scan provides suitable anatomical landmarks and allows computation of follicular volume, an important marker of maturity as corroborated by SPIM measurements (supplementary figure 1). A fly-by video of cross-sections of the entire ovary is shown in movie 1 (Frames: 160, Step Size: 0.1 mm, obtained at 720nm at 34.1˚C). Fast scanning protocols (~ 5 min/ ovarian sample) with 10 Hz laser pulsation was employed, the laser irradiation on the surface of ovaries is 12-20 mJ/ pulse (wavelength dependent). The values are below the maximum permissible limits (MPE) for *in vivo* small animal imaging.

Ovaries were scanned before (pre-injection) and after (post-injection) the BCB was injected. We observed a clear increase of signal along the walls of the follicles post-injection, as illustrated by figure 4.b, vis-à-vis the pre-injection image (figure 4.a). The test was repeated over 12 ovarian samples (~ 100 follicles). Two ovaries were selected for quantitative evaluation and their relative signal increase was calculated. Figure 4c shows box plots of normalized intensities

of 15 ROIs chosen in each ovary along the follicle walls for two independent ovarian samples. In both cases, intensity of optoacoustic signal from the post injection image was higher than pre-injection image of ovaries, considering the images were acquired at 690nm laser wavelength i.e. highest absorption of BCB in the probed optical spectrum. In the pre-injection sample, the follicles are barely visible, however the residual blood in bigger vessels shows up as bright contrast (figure. 4.a). Thus, we choose suitable ROI (around the follicles) instead of taking the mean intensity value of the images, to avoid erroneous quantification from the presence of residual blood. The spread of contrast values post-injection was higher compared to pre-injection, due to the different levels of hormones and follicular volumes. (figure. 4.b) The detailed scatter plot (supplementary figure 2) shows the intensities before and after injection of each ROI. Close observation revealed that some ovarian follicles show no significant changes in contrast even after injection, these are developing follicles that decolorize the BCB contrast. These BCB−ve follicles can thus be rejected, and oocytes are not extracted from them for further development.

Validation of MSOT imaging using histology and SPIM studies

The MSOT system used was limited to 150µm in-plane resolution [30], extendable to ~ 120 µm using pixel super-resolution methods [31]. This was optimal for visualizing BCB contrast within follicular masses, but fell short of visualizing the COCs. To validate our observations at higher resolution, a randomly chosen set of MSOT-analyzed ovarian follicles were cryosliced (figure 5.a) for examination using histological methods and SPIM. The insert (red) in figure 5.a, shows the chemically cleared oocyte, 5.b shows the reference MSOT image, 5.c shows the H&E stained image (20x) and 5.d shows the SPIM image of the intact follicle.

A state-of-the-art SPIM system [32] (supplementary figure 1.a) was fabricated in-house to enable ovarian follicular imaging. A wide range of individual follicles were extracted from two different sets of ovaries and all selected samples were imaged in their entirety, as their sizes matched the camera field of view (FOV). The SPIM imaging requires sample's transparency, which is achieved via a time-consuming chemical clearing protocol to render the samples free of optical scattering (see supplementary methods for details of the SPIM method). The high contrast-to-noise ratio and image resolution achieved by SPIM readily distinguished the different anatomical features (figure 5.d). We analysed the most relevant morphological features using the SPIM images, i.e. size of the developing COC and follicle wall thickness. The COC can be clearly seen attached to the inner follicle wall. COCs were detectable in approximately 70% follicles, and COC size varied between 40 μm and 110 μm (supplementary figure 1.b/ movie 2). Detection of COC as small as 40 μm is comparable to the resolution of histological analysis[33], and surpasses that of ultrasound biomicroscopy [34]. Histological sections obtained through cryoslicing (figure 5.a) and H&E stained microscopic images served as controls (figure 5.c).

In vitro embryo culture

We examined whether oocyte viability was harmed by laser irradiation from MSOT scanning and BCB staining. Nuclear maturation of each oocyte was scored by attainment of metaphase II, as judged by the presence of condensed chromosomes in an equatorial position and extrusion of the first polar body (figure 6). Nuclear maturation data (Table 1) showed no significant difference in nuclear maturation rate between MSOT-scanned and non-scanned control oocytes. The MSOT scanner provides a narrow, but sufficient band of wavelengths to identify signals from competent BCB (+) follicles and distinguish them from the developing follicles. This enabled suitable oocytes to be selected for *in vitro* embryo culture without disrupting follicle structure. To validate the

findings, we assessed the competence of oocytes to develop further by culture *in vitro*. Oocytes aspirated from MSOT-scanned ovaries were parthenogenetically activated to indicate developmental potential. Development was scored as the number of embryos consisting of two to eight equally-sized blastomeres 48 h after activation. No statistically significant difference was observed between MSOT-scanned BCB +ve oocytes and control BCB+ve oocytes (Table 1), indicating that MSOT scanning has no detectable detrimental effect. As expected, nuclear maturation and parthenogenetic activation rates were significantly higher in BCB+ve than BCB–ve oocytes, as reported in goats [35] and heifers[36]. The low nuclear maturation rate of BCB–ve oocytes could be due to incomplete or abnormal cytoplasmic maturation.

Table 1. Nuclear maturation and parthenogenetic activation

	MSOT scanned		**Control group**	
	BCB+ve	BCB-ve	BCB+ve	BCB-ve
Nuclear maturation (%)	85.52%±2.92	78.41%±3.91	86.48% ± 3.07	79.9%±3.82
Parthenogenetic activation (%)	88.91%±3.65	70.57%±3.28	87.98%±4.91	69.03% ±5.26

Expression of stress and apoptosis-related genes in BCB-MSOT scanned porcine COCs

Gene expression analysis of five genes (supplementary table 1) chosen for their roles in cell stress and apoptosis were conducted to determine whether BCB staining and irradiation from MSOT scanning is stressful to oocytes. Differential expression of the stress-associated gene *TP53* and three genes related to apoptosis, *BCL*, *BAK* (BCL2-antagonist/killer), and *CASP3* (caspase 3), was analyzed by quantitative real-time RT-PCR in two pools of 50 to 60 randomly-selected COCs from scanned and control ovaries without considering their developmental competence (Figure 7.a).

Three replicates were conducted for each experiment. Figure 7.b shows that no significant difference was detected in relative mRNA expression of *TP53*, *BCL*, *BAK* and *CASP 3* ($p<0.05$), between oocytes isolated from BCB-MSOT scanned and control ovaries. Studies in humans and mice have revealed a clear relationship between *in vitro* culture related stress and *TP53* expression in embryos[37]. *BCL XL, BAK* and *CASP3* are members of two important regulatory families involved in apoptosis. BCL XL and *BAK* are a pro-apoptotic members of the Bcl-2 family that induce oocyte apoptosis when cytoplasmic levels are elevated [38].

DNA fragmentation assay

TUNEL analysis to detect DNA fragmentation was carried out as a further indicator of cell stress and apoptosis, following the protocol described previously [39](figure 8. a-c). A TUNEL score was determined as the percentage of COCs showing signs of DNA fragmentation, as indicated by a fluorescent signal. There was no significant difference in TUNEL score between oocytes isolated from BCB-MSOT scanned ovaries (31.26% ± 4.23) and from control ovaries (30.11%± 2.97). Though it is not clear whether the BCB test could serve as an indirect marker of oocyte apoptosis, our investigation of the probable effect of MSOT scanning on oocyte quality revealed that it imposed no apparent stress on the oocyte. The average exposure time for each ovary was ~ 25 min, with maximal flux ~20 mJ cm^{-2} (per pulse) and average intensity of 200 mW cm^{-2} at the surface (at 750 nm). Although not directly relevant for our imaging experiments, these per-pulse energy levels and average power of the laser were below the MPE levels for human skin [40]. There exists no regulatory guideline for irradiation of internal organs or reproductive tissue, and researchers commonly determine damages by visual observation or cryoslicing extracted tissue. The histological and SPIM evaluations showed no physical damage to the tissue. Due to extended processing time and exposure of oocytes due to imaging, we also conducted the DNA

fragmentation checks. We found no evidence of DNA fragmentation in the cumulus layer in immature porcine COCs. This is consistent with a similar finding in cattle where no TUNEL signal was obtained in cumulus cells of immature oocytes[41]. Thus, the DNA fragmentation assay and relative mRNA expression of important apoptosis-related genes indicate that BCB-MSOT scanning does not cause stress to the oocytes.

Discussion and Conclusions

We describe a novel combination of ovarian follicle imaging with BCB as intra-vital contrasting medium using MSOT technology. The volumetric optoacoustic scanning (planar imaging plus Z-translation) provided suitable anatomical landmarks, and multi-wavelength acquisition allowed spectral resolution of the contrast agent (BCB). The anatomic scans using single wavelength optoacoustic images and 3D acquisitions distinctly show the follicular antrum and theca interna layers (figure 3, video 1), allowing individual follicles to be easily identified. The segmentation and volumetric evaluation of the follicles from anatomic data (as carried out in ultrasonic evaluation of ovaries in clinical cases) can also be achieved using the MSOT data [5,42]. However, such evaluations are beyond the scope of the current article; and are anyway redundant and insufficient in view of the availability of superior molecular information (BCB contrast) provided by MSOT.

Ovarian follicles were validated by a state-of-the-art SPIM system specifically designed for ovarian follicle imaging. Clearly distinguishable COCs protruding into the follicular antrum of several antral and Graafian follicles were measured at 40-110 µm, and their correlation with the

developmental stage of the follicles was as described by others [33] (supplementary figure 1). SPIM imaging coupled with the cryosection and histological (H&E stained) images provided a suitable measure to determine the efficacy of the BCB contrast enhanced MSOT imaging protocol.

The MSOT system has lower imaging resolution compared to microscopy but has the advantage of being non-destructive, unlike SPIM and histological analyses. The high spatial resolution and excellent contrast offered by BCB contrast-enhanced MSOT imaging provides quantitative anatomical information similar to that obtained by ultrasonic measurements commonly used in animal studies[33] and clinical practice[5]. Furthermore, the functional capability of MSOT as an imaging modality allows visualizing the presence (or absence) of BCB contrast without disrupting the follicle, opening up exciting new possibilities in molecular imaging for ART. Maintaining oocyte viability was one of the most important criteria for our study and defined the choice of BCB as a contrast medium and MSOT as a non-ionizing imaging modality. MSOT imaging added extra few hours to the processing of COC and in vitro culture. The RT-PCR and embryo development assay were done to see if the additional steps have any detrimental effect on the oocyte quality. However, we found no contra-indications. Parthenogenetic activation and embryo development indicated that the imaging was harmless and analysis of DNA fragmentation and expression of important apoptosis-related genes indicated no apparent damage to the oocytes. Our investigation provides further support for the use of BCB as a safe labelling agent for oocyte selection, and demonstrates the applicability of MSOT in *in vitro* embryo production.

There is immense scope for improving ovarian imaging techniques, as existing methods provide only crude information with questionable predictive value. Oocyte quality is certainly an important factor determining the outcome of ART procedures, but so far it has not been possible to test oocyte quality within a follicle. We therefore anticipate that a non-destructive method that reliably

predicts the quality of the developing oocyte inside a follicle will be of great benefit. As illustrated in the current article, an approach for functional oocyte and embryo assessment by ovarian imaging with the use of an exogenous contrast agent, can indeed be a key new technology for artificial reproduction.

The current study is a step beyond the conventionally practiced ultrasound guided antral follicle count and the proxy biochemical tests used for predicting ovarian reserve. The proposed methodology takes into account the quality, the competence and the developmental potential of the oocyte residing in the follicles within the ovary. Recent advancements in MSOT technology has allowed non-invasive assessment of intestinal wall [43], transvaginal imaging of ovaries [44], and transrectal imaging of prostrate [45]. These technological progress in system design will indeed be helpful in translating our imaging protocol to the clinics. Future development of the approach will open new dimensions in follicular imaging delivering useful anatomical, functional and molecular information without hampering the integrity of the follicle. Possible applications include diagnosis of follicular cysts, empty follicle syndrome, and developmental studies. The poor quality of retrieved oocytes due to improper timing of oocyte retrieval is an important factor in the relatively low success rate of human IVF. *In vivo* visualization of oocytes in situ could help practitioners to make informed decisions about timing oocyte retrieval.

Experimental Section

The materials and methods are detailed in the supplementary material. Additional results (supplementary table 1 and figures 1-2) supporting the claims made in the manuscript are included in the supplementary material.

Acknowledgements

We thank SJ Ford and R. Phaltane for the productive discussions and V. Gujrati for a close reading of the manuscript. We would like to thank Steffen Löbnitz for his help in collecting samples.

Author contributions

RD and SM jointly conceived the idea of the imaging protocol, designed and conducted experiments; they contributed equally to the project. SM conducted the optoacoustic (OA) measurement, and developed/improved the imaging and image analysis algorithms. RD participated in the OA studies, and was responsible for *in vitro* embryo cultures and biological assays. HCAL and DR developed, and conducted the experiments using the SPIM system. RD, SM and HCAL executed the histological imaging and validation steps. DR, AK AS and TR critically reviewed and validated the findings. AS and DR supported and supervised the project. RD, SM, AK, DR participated in writing and revising the manuscript.

Compliance with Ethical Standards:

Funding: RD and SM acknowledges DAAD (PhD Scholarships) for the funding support.

Conflict of Interest: The authors declare no conflict of interest.

Ethical approval: All procedures involving animal care and experimentation were conducted according to the guidelines of Helmholtz Zentrum München and the government of Upper Bavaria and complied with German federal and international laws and regulations.

This article does not contain any studies with human participants performed by any of the authors.

References

1. Tal R, Seifer DB. 2017 Ovarian reserve testing: a user's guide. *Am. J. Obstet. Gynecol.* (doi:10.1016/j.ajog.2017.02.027)

2. Tal R, Seifer DB. 2013 Potential mechanisms for racial and ethnic differences in

antimüllerian hormone and ovarian reserve. *Int. J. Endocrinol.* (doi:10.1155/2013/818912)

3. Fransisco K. 2016 Assisted Reproductive Technology. In *Encyclopedia of Family Studies*, John Wiley & Sons, Inc. (doi:10.1002/9781119085621.wbefs435)

4. S. P, R. J. 2013 Follicle Detection and Ovarian Classification in Digital Ultrasound Images of Ovaries. In *Advancements and Breakthroughs in Ultrasound Imaging* (ed GPP Gunarathne), InTech.

5. Krivanek A, Sonka M. 1998 Ovarian ultrasound image analysis: follicle segmentation. *Med. Imaging, IEEE Trans.* **17**, 935–944. (doi:10.1109/42.746626)

6. Zheng H, Chen X-L, Zhu C-Q, Li D-H, Chen Q-Y, Xu J-G. 2000 Brilliant cresyl blue as a new red region fluorescent probe for determination of nucleic acids. *Microchem. J.* **64**, 263–269. (doi:10.1016/S0026-265X(00)00015-1)

7. Pereira GR, Lorenzo PL, Carneiro GF, Bilodeau-Goeseels S, Kastelic JP, Esteller-Vico A, Lopez-Bejar M, Liu IKM. 2014 Selection of developmentally competent immature equine oocytes with brilliant cresyl blue stain prior to in vitro maturation with equine growth hormone. *Zygote* **22**, 500–504. (doi:10.1017/S096719941200072X)

8. Manjunatha BM, Gupta PSP, Devaraj M, Ravindra JP, Nandi S. 2007 Selection of developmentally competent buffalo oocytes by brilliant cresyl blue staining before IVM. *Theriogenology* **68**, 1299–1304. (doi:10.1016/j.theriogenology.2007.08.031)

9. Katska-Ksiazkiewicz L, Opiela J, Ryńska B. 2007 Effects of oocyte quality, semen donor and embryo co-culture system on the efficiency of blastocyst production in goats. *Theriogenology* **68**, 736–744. (doi:10.1016/j.theriogenology.2007.06.016)

10. Su J, Wang Y, Li R, Peng H, Hua S, Li Q, Quan F, Guo Z, Zhang Y. 2012 Oocytes selected using BCB staining enhance nuclear reprogramming and the in vivo development of SCNT embryos in cattle. *PLoS One* **7**, e36181. (doi:10.1371/journal.pone.0036181)

11. Stanton RC. 2012 Glucose-6-Phosphate Dehydrogenase, NADPH, and Cell Survival. *IUBMB Life* **64**, 362–369. (doi:10.1002/iub.1017)

12. Mirshamsi SM, KaramiShabankareh H, Ahmadi-Hamedani M, Soltani L, Hajarian H, Abdolmohammadi AR. 2013 Combination of oocyte and zygote selection by brilliant

cresyl blue (BCB) test enhanced prediction of developmental potential to the blastocyst in cattle. *Anim. Reprod. Sci.* **136**, 245–251. (doi:10.1016/j.anireprosci.2012.11.002)

13. Razansky D, Distel M, Vinegoni C, Ma R, Perrimon N, Köster RW, Ntziachristos V. 2009 Multispectral opto-acoustic tomography of deep-seated fluorescent proteins in vivo. *Nat. Photonics* **3**, 412–417. (doi:10.1038/nphoton.2009.98)

14. Mandal S, Dean-Ben XL, Burton NC, Razansky D. 2015 Extending biological imaging to the fifth dimension: Evolution of volumetric small animal multispectral optoacoustic tomography. *IEEE Pulse* **6**, 47–53. (doi:10.1109/MPUL.2015.2409103)

15. Ripoll J, Koberstein-Schwarz B, Ntziachristos V. 2015 Unleashing Optics and Optoacoustics for Developmental Biology. *Trends Biotechnol.* **33**, 679–691. (doi:10.1016/j.tibtech.2015.08.002)

16. Ermolayev V, Dean-Ben XLXL, Mandal S, Ntziachristos V, Razansky D. 2015 Simultaneous visualization of tumour oxygenation, neovascularization and contrast agent perfusion by real-time three-dimensional optoacoustic tomography. *Eur. Radiol.* **26**, 1–9. (doi:10.1007/s00330-015-3980-0)

17. Viator JA, Sutovsky P, Weight RM. 2008 Detection of dilute sperm samples using photoacoustic flowmetry. In *Photons Plus Ultrasound: Imaging and Sensing 2008: The Ninth Conference on Biomedical Thermoacoustics, Optoacoustics, and Acousto-optics*, (doi:10.1117/12.764105)

18. Tzoumas S, Deliolanis N, Morscher S, Ntziachristos V. 2013 Un-mixing Molecular Agents from Absorbing Tissue in Multispectral Optoacoustic Tomography. *IEEE Trans. Med. Imaging* **33**, 48–60. (doi:10.1109/TMI.2013.2279994)

19. Mandal S, Dean-Ben XL, Razansky D. 2016 Visual Quality Enhancement in Optoacoustic Tomography Using Active Contour Segmentation Priors. *IEEE Trans. Med. Imaging* **35**, 2209–2217. (doi:10.1109/TMI.2016.2553156)

20. Ntziachristos V, Razansky D. 2010 Molecular imaging by means of multispectral optoacoustic tomography (MSOT). *Chem. Rev.* **110**, 2783–2794. (doi:10.1021/cr9002566)

21. Ding L, Luís Deán-Ben X, Lutzweiler C, Razansky D, Ntziachristos V. 2015 Efficient

non-negative constrained model-based inversion in optoacoustic tomography. *Phys. Med. Biol.* **60**, 6733–6750. (doi:10.1088/0031-9155/60/17/6733)

22. Prakash J, Mandal S, Razansky D, Ntziachristos V. 2019 Maximum entropy based non-negative optoacoustic tomographic image reconstruction. *IEEE Trans. Biomed. Eng.* , 1–1. (doi:10.1109/TBME.2019.2892842)

23. Mandal S, Nasonova E, Deán-Ben XL, Razansky D. 2014 Optimal self-calibration of tomographic reconstruction parameters in whole-body small animal optoacoustic imaging. *Photoacoustics* **2**, 128–136. (doi:10.1016/j.pacs.2014.09.002)

24. Luke GP, Nam SY, Emelianov SY. 2013 Optical wavelength selection for improved spectroscopic photoacoustic imaging. *Photoacoustics* **1**, 36–42. (doi:10.1016/j.pacs.2013.08.001)

25. Mohammadi-Sangcheshmeh A, Soleimani M, Deldar H, Salehi M, Soudi S, Hashemi SM, Schellander K, Hoelker M. 2012 Prediction of oocyte developmental competence in ovine using glucose-6-phosphate dehydrogenase (G6PDH) activity determined at retrieval time. *J. Assist. Reprod. Genet.* **29**, 153–158. (doi:10.1007/s10815-011-9625-6)

26. Fuenzalida Werner JP *et al.* 2020 Challenging a Preconception: Optoacoustic Spectrum Differs from the Optical Absorption Spectrum of Proteins and Dyes for Molecular Imaging. *Anal. Chem.* (doi:10.1021/acs.analchem.0c01902)

27. Nascimento JMPJMP, Dias JMB, Bioucas-Dias JM. 2005 Vertex component analysis: A fast algorithm to unmix hyperspectral data. *IEEE Trans. Geosci. Remote Sens.* **43**, 898–910. (doi:10.1109/TGRS.2005.844293)

28. Viswanath PSS, Weiser T, Chintala P, Mandal S, Dutta R. 2016 Grading of mammalian cumulus oocyte complexes using machine learning for in vitro embryo culture. In *2016 IEEE-EMBS International Conference on Biomedical and Health Informatics (BHI)*, pp. 172–175. IEEE. (doi:10.1109/BHI.2016.7455862)

29. Borup R, Thuesen LL, Andersen CY, Nyboe-Andersen A, Ziebe S, Winther O, Grøndahl ML. 2016 Competence Classification of Cumulus and Granulosa Cell Transcriptome in Embryos Matched by Morphology and Female Age. *PLoS One* **11**, e0153562.

(doi:10.1371/journal.pone.0153562)

30. Razansky D, Buehler A, Ntziachristos V. 2011 Volumetric real-time multispectral optoacoustic tomography of biomarkers. *Nat. Protoc.* **6**, 1121–9. (doi:10.1038/nprot.2011.351)

31. He H, Mandal S, Buehler A, Dean-Ben XLL, Razansky D, Ntziachristos V. 2016 Improving Optoacoustic Image Quality via Geometric Pixel Super-Resolution Approach. *IEEE Trans. Med. Imaging* **35**, 812–818. (doi:10.1109/TMI.2015.2497159)

32. Lin HCAH-CA *et al.* 2016 Advancing ovarian folliculometry with selective plane illumination microscopy. *Sci. Rep.* **6**, (Accepted for publication). (doi:10.1038/srep38057)

33. Griffin J, Emery BR, Huang I, Peterson CM, Carrell DT. 2006 Comparative analysis of follicle morphology and oocyte diameter in four mammalian species (mouse, hamster, pig, and human). *J. Exp. Clin. Assist. Reprod.* **3**, 2. (doi:10.1186/1743-1050-3-2)

34. Pfeifer LFM, Siqueira LGB, Adams GP, Pierson RA, Singh J. 2012 In vivo imaging of cumulus-oocyte-complexes and small ovarian follicles in cattle using ultrasonic biomicroscopy. *Anim. Reprod. Sci.* **131**, 88–94. (doi:10.1016/j.anireprosci.2012.02.014)

35. Rodríguez-González E, López-Béjar M, Velilla E, Paramio MT. 2002 Selection of prepubertal goat oocytes using the brilliant cresyl blue test. *Theriogenology* **57**, 1397–1409. (doi:10.1016/S0093-691X(02)00645-3)

36. Pujol M, López-Béjar M, Paramio MT. 2004 Developmental competence of heifer oocytes selected using the brilliant cresyl blue (BCB) test. *Theriogenology* **61**, 735–744. (doi:10.1016/S0093-691X(03)00250-4)

37. Chandrakanthan V, Li A, Chami O, O'Neill C. 2006 Effects of in vitro fertilization and embryo culture on TRP53 and Bax expression in B6 mouse embryos. *Reprod. Biol. Endocrinol.* **4**, 61. (doi:10.1186/1477-7827-4-61)

38. Morita Y, Tilly JL. 1999 Oocyte apoptosis: like sand through an hourglass. *Dev. Biol.* **213**, 1–17. (doi:10.1006/dbio.1999.9344)

39. Rahul Dutta, Shun Li, Konrad Fischer, Alexander Kind, Tatiana Flisikowska, Krzysztof Flisikowski OR and AS, Dutta R, Li S, Fischer K, Kind A, Flisikowska T, Flisikowski K,

Rottmann O, Schnieke A. 2015 Non-invasive assessment of porcine oocyte quality by supravital staining of cumulus–oocyte complexes with lissamine green B. *Zygote* **FirstView**, 1–10. (doi:10.1017/S0967199415000349)

40. ANSI. 2014 *American National Standard for Safe Use of Lasers*. See http://webstore.ansi.org/RecordDetail.aspx?sku=ANSI+Z136.1-2014.

41. Yuan YQ, Van Soom A, Leroy JLMR, Dewulf J, Van Zeveren A, de Kruif A, Peelman LJ. 2016 Apoptosis in cumulus cells, but not in oocytes, may influence bovine embryonic developmental competence. *Theriogenology* **63**, 2147–2163. (doi:10.1016/j.theriogenology.2004.09.054)

42. Kwee J, Elting ME, Schats R, McDonnell J, Lambalk CB. 2007 Ovarian volume and antral follicle count for the prediction of low and hyper responders with in vitro fertilization. *Reprod. Biol. Endocrinol.* **5**, 9. (doi:10.1186/1477-7827-5-9)

43. Knieling F *et al.* 2017 Multispectral Optoacoustic Tomography for Assessment of Crohn's Disease Activity. *N. Engl. J. Med.* **376**, 1292–1294. (doi:10.1056/NEJMc1612455)

44. Salehi HS, Li H, Merkulov A, Kumavor PD, Vavadi H, Sanders M, Kueck A, Brewer MA, Zhu Q. 2016 Coregistered photoacoustic and ultrasound imaging and classification of ovarian cancer: ex vivo and in vivo studies . *J. Biomed. Opt.* (doi:10.1117/1.jbo.21.4.046006)

45. Kothapalli SR *et al.* 2019 Simultaneous transrectal ultrasound and photoacoustic human prostate imaging. *Sci. Transl. Med.* (doi:10.1126/scitranslmed.aav2169)

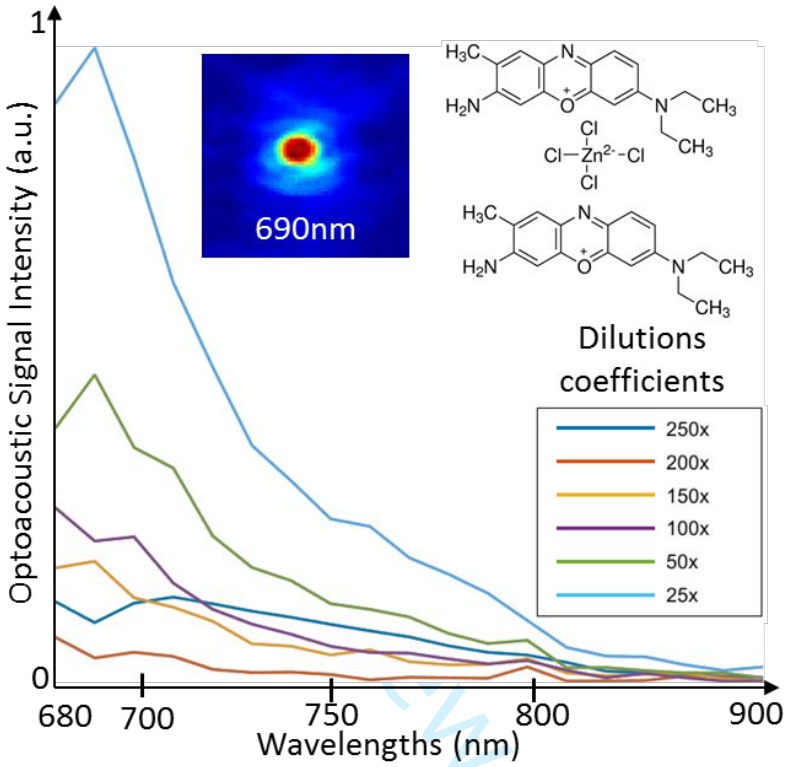

Figure 1. Wavelength dependent optoacoustic signal extinction curve for BCB: The optoacoustic signal responses are measured at several pre-injection dilution coefficients (x =13mM stock solution of BCB/DPBS) using the MSOT (cross-sectional) imaging at varying wavelengths. The BCB solution was perfused through a transparent fine bore polyurethane tubing (0.86mm ID and 1.27mm OD) embedded inside a scattering agar block (7% intralipid by volume). The signal values were determined by fitting an ROI and computing the mean image intensity across the ROI, each for corresponding wavelengths (20WLs were recorded) and dilution coefficients. A representative reconstructed an image (WL 690) is shown in an insert.

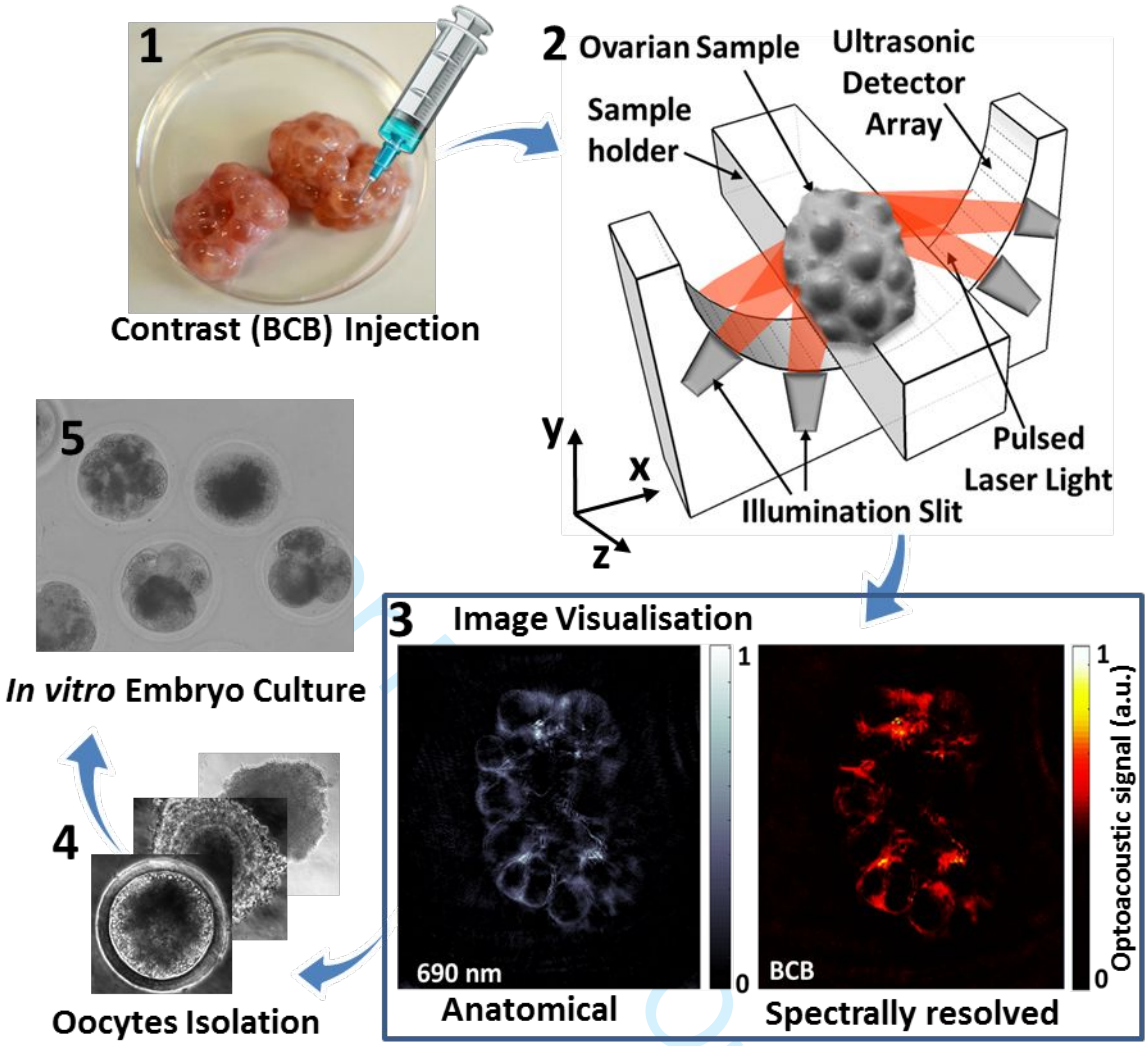

Figure 2. Protocol for ovarian imaging: (1) BCB was injected into the ovarian follicles using a ultrafine needle. (2) After BCB injection ovaries were imaged using MSOT. (3) Single wavelength (690 nm) image of BCB contrast enhanced ovarian follicles are shown in anatomical reference image, and the contrast from BCB molecules is spectrally resolved through a blind unmixing process using 5 wavelengths (4) Following MSOT imaging oocytes were isolated by aspiration and kept for further in vitro culture and analysis. (5) The final stage shows successful formation of the embryo from the isolated oocytes extracted from the BCB+ MSOT scanned ovarian follicles.

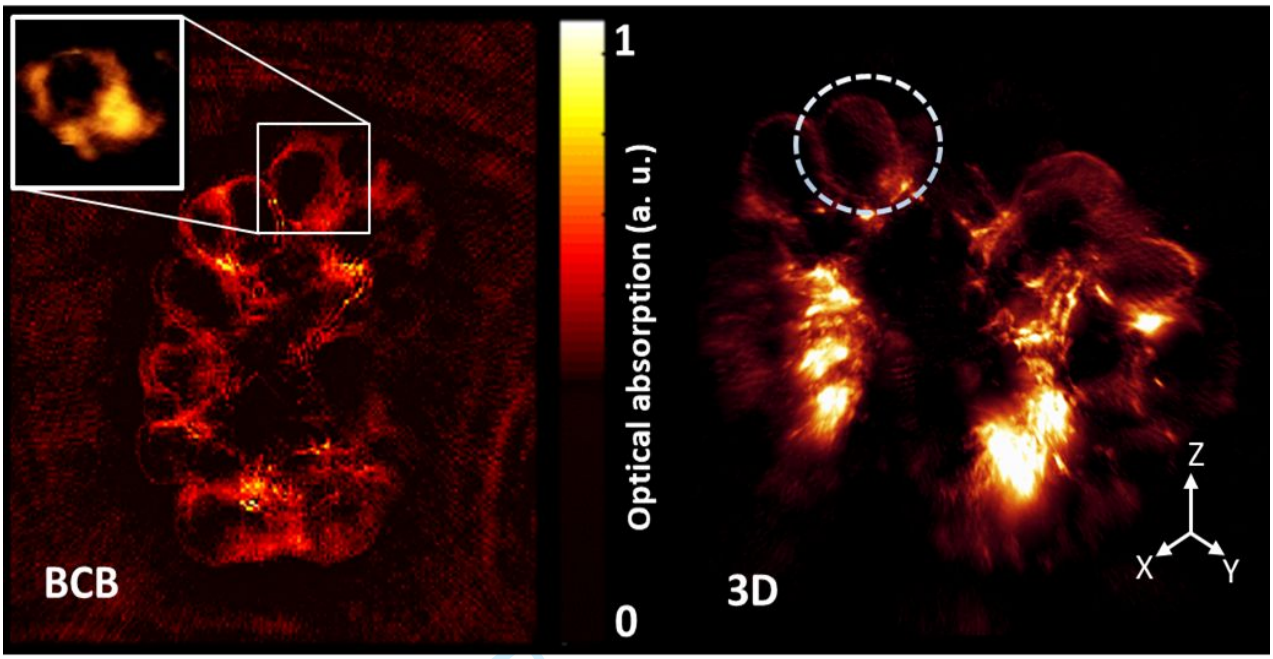

Figure 3. The unmixed BCB channel obtained by using 5 wavelengths(a), the insert shows the original position of the isolated oocyte, and a zoomed in 3D volume rendered version of the selected single oocyte. (b) 3D rendering of entire ovary obtained using z-slacking and fast scanning protocols (~ 5 min/ ovarian sample @ 10 Hz laser pulsation), approximate position of a single viable oocyte is marked.

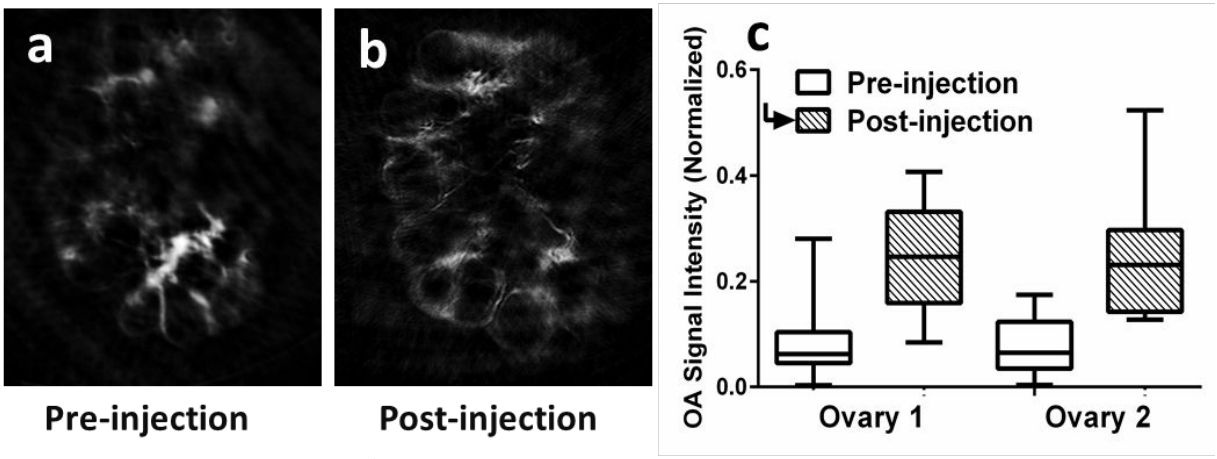

Figure 4. Scan of (intact) ovaries *ex-vivo* before (a) and after (b) injection of BCB (100x diluted 13Mm stock solution) is shown. The post-injection images (normalized) of the ovaries show an increase in relative contrast values. The box-plots of contrast values for two ovaries, before and after the injection are shown (c). Fifteen (15) data-points in each ovary was chosen for evaluation. Supplementary figure 2 shows the scatter plot of the data-points (both before and after injection) for each of the follicles in individual ovaries.

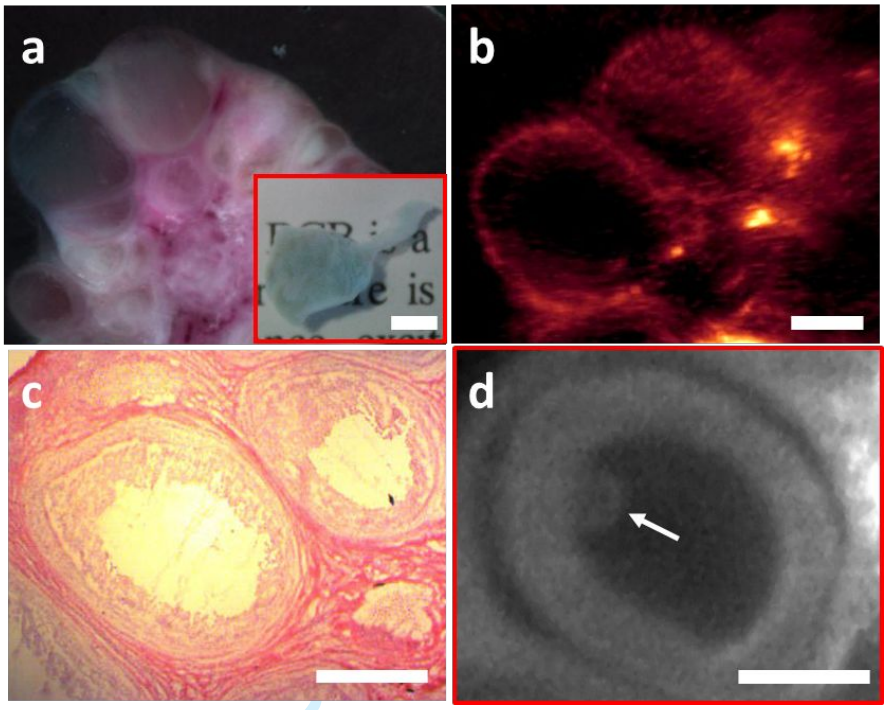

Figure 5. The cryosliced image of BCB+ porcine ovary (a), and the optoacoustic image of the selected ovarian section is shown (b). The histological evaluation was done using H&E stains (c), and validated using the SPIM imaging (d). Insert in (a) shows an isolated follicle which was cleared and imaged using SPIM to obtain the corresponding anatomy for validation (d), the arrow points to the attached COC. [Scalebars ≈1 mm]

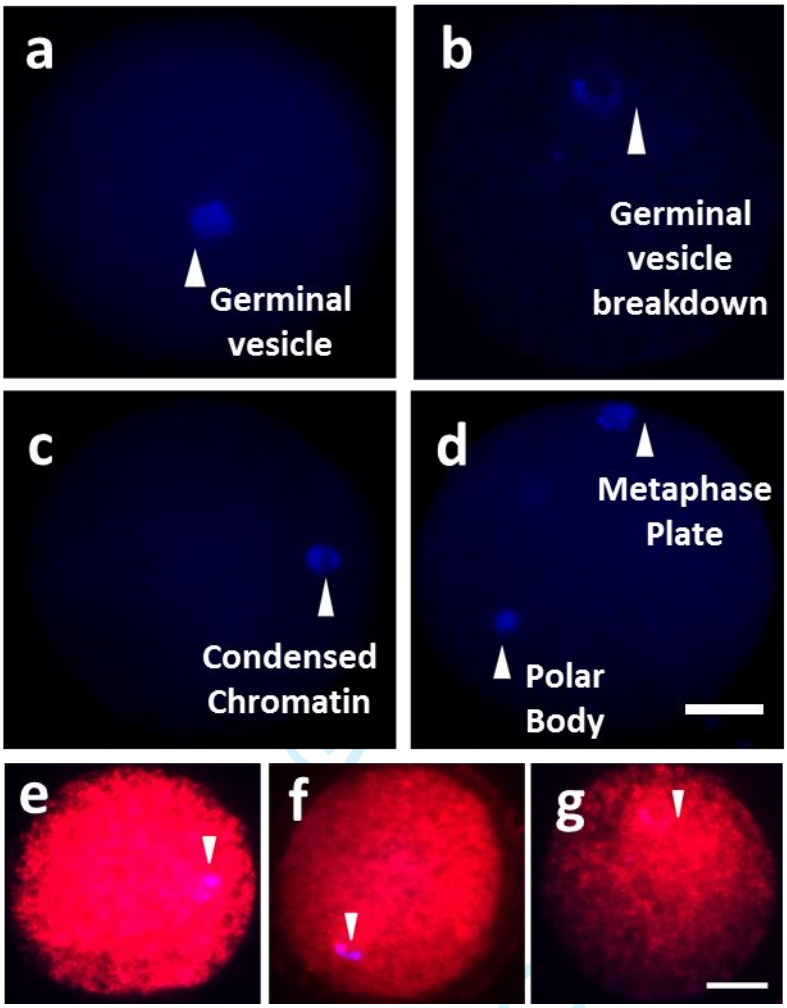

Figure 6. Progression of BCB stained oocytes through different stages of maturation: (a) Immature oocyte (b) Germinal Vesicle breakdown stage (c) appearance of first polar body and (d) Mature oocyte with visible polar body and metaphase plate. Mitochondrial distribution of (e) BCB+ ve oocytes showing uniform distribution with polar body and metaphase plate, (f) a control oocyte showing uniform distribution with polar body and metaphase plate and (g) BCB – ve oocyte arrested at germinal vesicle breakdown stage with non-uniform mitochondrial distribution. All scale bars indicate 100 µm.

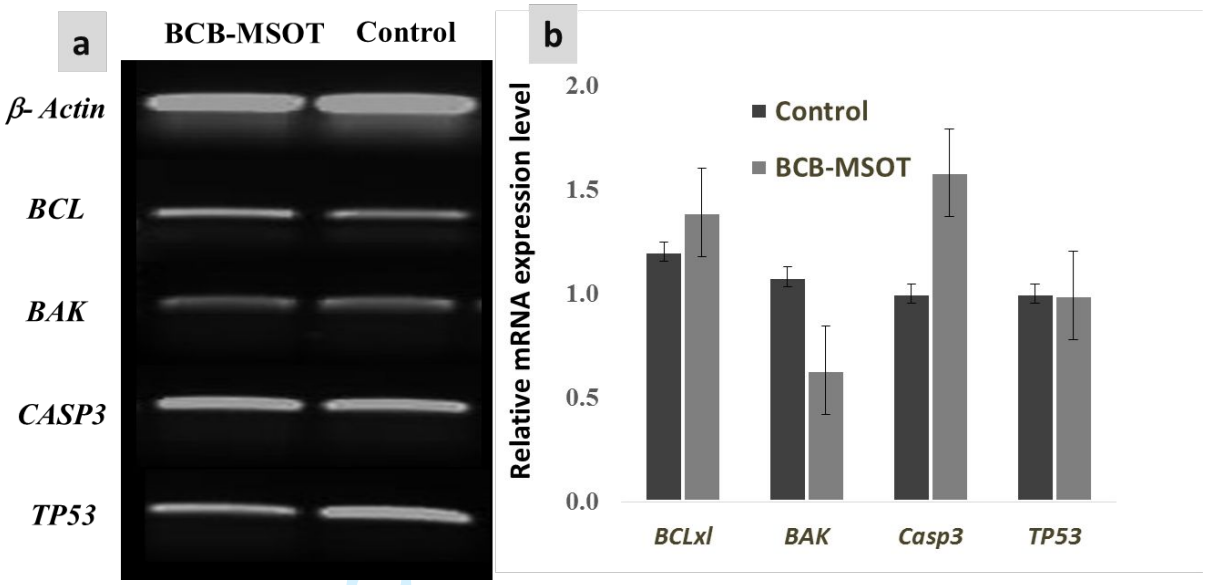

Figure 7. . The Reverse transcription PCR of (a) apoptosis associated and stress associated genes in MSOT scanned oocytes (exposure 5-20 mins). The panel (b) shows the statistical significances for tests conducted with ß-Actin, BCL BAK and TP53 -- no significant DNA damage due to BCB and/or MSOT scanning is observed.

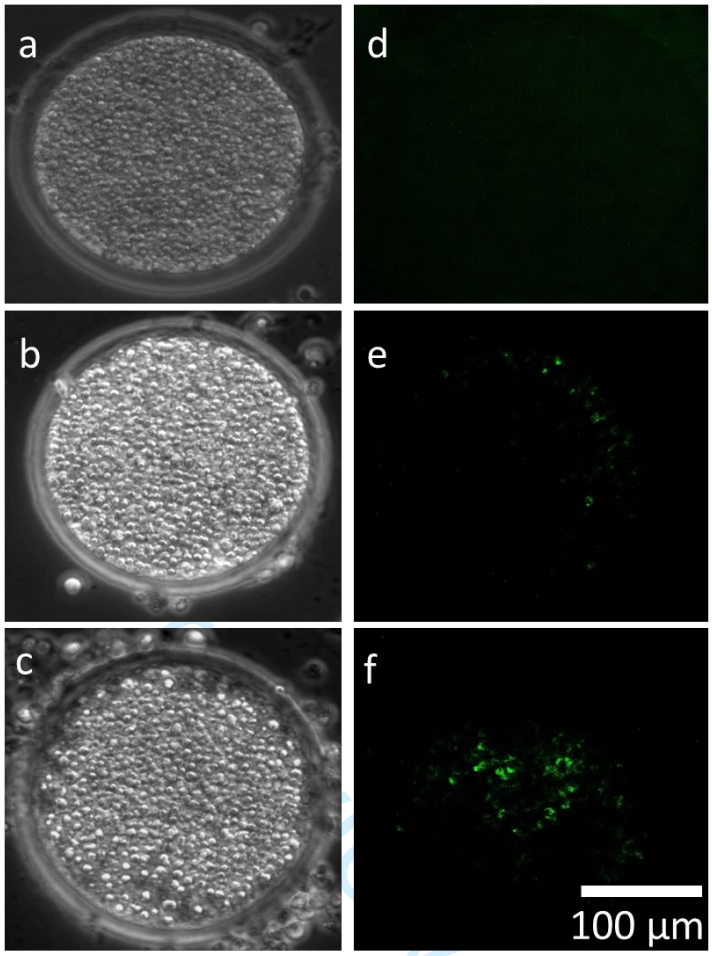

Figure 8. DNA fragmentation detection (bright-field images) by TUNEL assay (a) Porcine oocyte with no detectable DNA fragmentation, (b) BCB +ve porcine oocyte with DNA fragmentation, and (c) control oocyte with DNA fragmentation. The corresponding fluorescent channel images of (a-c) are shown (d-f) on the same scale.

Supplementary Information

Material and methods

1.1. BCB dilution and spectrum calculation

BCB contains a primary amine on the benzenoid structure (Φ-NH_2), a tertiary amine (R_3N) and a quaternary ammonium salt (R_4N+), the chemical structure[1] is included in Fig 1b (Zhang et. al, Appl Spect, 98). The optical and optoacoustic response of BCB was characterized using spectroscopic measurements (Ocean optics USB4000-FL, Bandwidth: 351-1043nm) and direct optoacoustic measurements with different concentrations of BCB diluted in PBS. Spectroscopic measurements show the absorption peak at 620 nm. However, this wavelength cannot be used for optoacoustic a measurement because the laser is optimized in the range 680-900 nm for maximum tissue penetration. We measured the optoacoustic spectrum by placing a fine bore polyethylene tubing (0.86mm ID and 1.27mm OD) embedded within a diffusing agar block (for uniform illumination) and perfusing BCB solutions at six different concentrations. The stock solutions (1 M) were diluted to achieve the desired concentration of 13mM. We probed different dilutions of this base concentration to find the correct usable concentration in tissue. The signals were acquired by an array of 256 detectors (averaged signal over 50 acquisitions) using 10 wavelengths (680nm -730nm at intervals of 10nm → 6 wavelengths, 730 nm, 760 nm, 800 nm, 850 nm, and 900 nm). The images were reconstructed using IMMI method (see section 1.2 for explanation) with non-negative constrains. The signals were normalized for laser power over all 20 wavelengths and the lumen of the tubing was segmented. Thereafter the spectral signal amplitude was obtained as an average of the integral intensity value across the segmented lumen and plotted for different concentrations of solution (Figure 1).

1.2 MSOT Imaging Protocol

Porcine ovaries were brought from a slaughterhouse to the laboratory, within one hour of collection, in a temperature-controlled box maintained at a temperature of 39˚C. Ovaries were thoroughly washed with pre-warmed (39˚C) Dulbecco's phosphate-buffered saline (DPBS) solution containing 0.1% polyvinyl alcohol and penicillin, streptomycin solution. Then, 50 µl samples of 13 mM BCB were carefully injected into 4-6 mm follicles using a fine 29 G needle (figure 2.a). The ovary was then fixed using a polythene film inside the MSOT scanner (Figure 2b).

Imaging of explanted ovaries was performed by cross-sectional optoacoustic acquisition geometry using a commercial small animal multispectral optoacoustic tomography (MSOT) scanner (Model: MSOT256-TF, iThera Medical GmbH, Munich, Germany). The scanning system consisted of a custom-made 256-element array of cylindrically-focused piezocomposite transducers with 5 MHz central frequency for simultaneous acquisition of the signals generated with each laser pulse. The transducer array covered an angle of approximately 270^0 and had a radius of curvature of 40 mm. Light excitation was provided with the output laser beam from a wavelength-tunable optical parametric oscillator (OPO)-based laser shaped to attain ring-type uniform illumination on the surface of the phantoms by means of a custom-made fiber bundle. Detected optoacoustic signals were simultaneously digitized at 40 Mega samples per second. The scanner was capable of rendering 10 cross-sectional images per second, but here the images were averaged 10 times in order to improve SNR performance in acquiring cross sections of the entire ovary. The acquired

signals were initially band-pass filtered with cut-off frequencies between 0.1 and 7 MHz to remove low-frequency offsets and high-frequency noise, and subsequently, input to a reconstruction algorithm rendering a cross-sectional distribution of the optical absorption.

The acquired images were reconstructed with the exact numerical model-based reconstruction algorithm[2], termed interpolated-matrix-model inversion (IMMI). The choice of IMMI was motivated by the need to have more quantitative optoacoustic reconstructions by taking into account the various experimental imperfection, retaining frequency information and mitigating artifacts, which are characteristic of the named class of algorithms. It is based on a least-squares minimization between the measured pressure at a set of locations and instants (expressed in a vector form as$\mathbf{p}$) and the equivalent theoretical pressure predicted by a linear model obtained from a discretization of the optoacoustic forward solution. Optical absorption at the pixels of the ROI, expressed as vector form$\mathbf{F}$, was calculated as follows

$$\mathbf{F} = \text{argmin}_{\mathbf{f}} \|\mathbf{Af} - \mathbf{p}\|^2 + \lambda^2 \|\mathbf{Lf}\|^2,$$

where A is the linear operator (or model matrix) mapping the optical absorption to the acoustic pressure. Standard Tikhonov regularization was employed to minimize high-frequency noise in the inversion process, which is particularly beneficial in presence of limited view problems. The matrix L represents a high-pass filter operation as described by Dean-Ben *et. al* [3]. The model-based inversion procedure can be further modified to account for speed-of-sound variations in the medium or to minimize artefacts due to internal reflections in case these cause undesired distortion in the images. In the current implementation, the computational time of model-based reconstruction was approximately 1.28 s in an Intel Core2 Duo CPU E8400 operating at 3.00 GHz and with 8 GB of RAM and was accelerated with GPU-based processing. We employed a grid of

200x200 pixels corresponding to a field of view of 25 mm x 25 mm (125 μm pixel size), which is adapted to the actual resolution of the system [4].

The ovarian images are obtained ex- vivo, they are extremely noisy and have low intrinsic contrast. To combat the situation and improve quantitative imaging performance we used non-negative constrained IMMI methods [5,6], which are more accurate but computationally expensive.

1.3 Spectral unmixing to identify BCB contrast

The MSOT is capable of selectively quantifying the distribution of specific biomarkers using multispectral information. We used a vertex component analysis (VCA) based fast blind unmixing method to map the distribution of BCB[7]. Since the internal molecular composition of fluid inside the follicles was not spectrally evaluated, the problem was treated mathematically as a two object problem – the tissue and the BCB contrast. Thus, in our approach, we unmixed specifically for the presence of BCB within the ovarian follicle, given that the presence of BCB+ structure helped identify the competent follicles. The VCA based spectral unmixing method was able to arbitrarily identify two channels and display the corresponding spectrum. The spectra were then matched with the optoacoustic spectrum of BCB experimentally measured and mapped to the corresponding tissue components and the BCB channel. For the mathematical formulation of the method used and its efficacy is given by Deán-Ben, X. Luís, et al (2014).

1.4 Validation of imaging using SPIM and histological evaluations

The MSOT equipment has a limited resolution (150 μm), so to validate MSOT images at higher resolution, randomly selected MSOT-scanned ovaries were subjected to SPIM analysis. A state-of-the-art SPIM system with an axial resolution of 11 μm was built in-house to optimally support imaging of ovarian follicle specimens (supplementary figure 3). The light source was an 80 mW

continuous wave DPSS laser at 670 nm (Frankfurt laser company, Germany), with a beam quality factor M^2=1.10. A 5X telescope system was used to expand the beam diameter to 10 mm to allow excitation of the full width of the ovary samples. A beam splitter was used to divide the main beam to allow double-sided illumination and reduce effects of light attenuation due to absorption and scattering when imaging through large samples.

Supplementary Figure 3a shows a side-view of the SPIM system. Thin sheets of light were generated using cylindrical lenses with focal lengths of 40 mm. The light sheets were oriented horizontally, with the sample centered at the beam waist. To capture 2D fluorescent images, a 5-MP scientific complementary metal oxide semiconductor (sCMOS) camera (Model: pco.edge, PCO AG, Kelheim, Germany) was placed directly above the sample, facing downwards. The high-end scientific camera allows acquisition of up to 100 frames per second with 2560 x 2160 pixel resolution and high sensitivity supported by a dynamic range of 14 bits and 1.0 e- readout noise. An EC Epiplan-Neofluar objective (Zeiss, Germany) with a magnification of 2.5X and an NA of 0.06 was used because it provided a large working distance of 35 mm, and 220 μm depth of field. Fluorescence signals were filtered using a 716/40 fluorescence filter (Chroma, USA), and a tube lens used to relay the fluorescent image into the camera. The imaging system was characterized using line pair targets, and determined to have an effective field-of-view (FOV) of 10x9 mm with <6 μm lateral resolution. The axial resolution was found to be 17 μm at the beam waist expanding to about 60 μm at 3 mm distance from the center of the FOV.

The Murray's clear protocol was used for chemical clearing of the samples. Follicles were dehydrated using 50%, 80%, and 100% ethanol for 12 hours each, repeating the last step twice. The samples were then cleared in 2:1 benzyl alcohol/ benzyl benzoate (BABB) solution for 6 hours.

Samples were fixed on a holder and placed inside the sample chamber. A linear motorized stage (Thorlabs, USA) was used to translate the chamber vertically, allowing different planes to be excited by the light sheet. Rapid translation enabled stacks of up to 600 cross-sectional SPIM images to be collected within two minutes. During imaging, the sample chamber was filled with BABB solution to match the refractive index of the medium to the sample, avoiding image distortion. A glass sample chamber was used to avoid reaction with BABB. Image analyses to extract morphological measurements were carried out using ImageJ software.

1. 5 Quantitative real-time PCR

To assess the effect of MSOT on oocyte viability, scanned and non-scanned control ovaries were transferred to the laboratory for further culture; transfer was made within 2 hours and temperature maintained at 39^0 C. BCB-infused follicles of 3-8mm diameter were aspirated using a vacuum suction machine 18-gauge needle(figure 1 d). Oocytes were cultured at 39^0 C under 5% CO_2 in the air and maximum humidity for 46 h. After 46 h of IVM, the nuclear maturation rate was calculated. Oocyte developmental potential was assessed by parthenogenetic activation by incubating in IVM medium containing 5 µM Ca-ionophore A23187 (C7522) for 5 min at 39^0C under 5% CO_2 in the air. After activation, oocytes were cultured in 500 µl porcine zygote medium (PZM 5 IFP) in 4 well dishes (Nunc GmbH, Co.KG, Germany) at 39^0C in 5% CO_2 in air for 7 days. Embryo development was observed microscopically and cleavage assessed 48 h post-activation (figure 1 e).

The relative mRNA expression of apoptosis-related genes was evaluated by quantitative RT-PCR of groups of 50 to 60 COCs aspirated from MSOT -scanned and non-scanned control ovaries. Total RNA was isolated using an RNeasy Mini Kit (Qiagen, Europe) according to the manufacturer's instructions. Sample purity was assessed using the A260/A280 nm ratio with

expected values between 1.8 and 2.0, RNA samples were treated with TURBO DNA-free™ Kit (Life Technologies) to remove genomic DNA. Reverse-transcription reactions were performed with 0.5–1 μg total RNA using the SuperScript® III First-Strand Synthesis System for RT-PCR (Life Technologies) and random hexamer as a primer, according to the manufacturer's instructions. For each sample, negative controls lacking reverse transcriptase were prepared using the identical procedure. Primers for *BAK*, *CASP3*, *BCL XL* , *TP53*, and a housekeeping gene *ACTB* (beta-actin) were designed using 'Primer3' software. The predicted sizes of amplified fragments are listed in Supplementary Table 2. Real-time PCR amplification was conducted using an ABI 7300 real-time PCR System (Applied Biosystems). A KAPA SYBR FAST q PCR Kit (Kapa Biosystems) was used to provide real-time quantification of the amplified products. Three replicates of each reaction were measured and the mRNA level of each sample was normalized to that of β actin. The relative levels of mRNA were analyzed by the ΔΔCt method.

1. 6 DNA fragmentation assay

The TUNEL (Terminal deoxynucleotidyl transferase-mediated dUTP nick end labelling) procedure was used to fluorescein-dUTP label 3'-OH ends of DNA fragments generated by apoptosis, allowing detection of apoptotic cells by fluorescence microscopy. Fixed and permeabilised oocytes were subjected to the TUNEL assay procedure using an in situ apoptosis detection kit (Takara Bio INC., Japan) according to the manufacturer's instructions. COCs were fixed for 30 minutes at room temperature in PBS (pH 7.4), permeabilised for 5 min on ice in permeabilisation buffer, and then washed once in PBS in preparation for the TUNEL procedure. COCs were incubated with terminal transferase and labelled nucleotide solution in a humidified, sealed chamber in the dark at 37ºC for 1 h. Before observation the slides were overlaid with a cover slip and the edges sealed with quick drying nail polish. The slides were evaluated using an

epifluorescence microscopy (Green excitation filter and Carl Zeiss). Oocyte showing discrete pinpoint fluorescent green signals were judged to be positive for DNA fragmentation. The apoptosis score was expressed as a percentage of the total.

1. 7 Statistical analysis

The statistical data was analyzed using GraphPad Prism (GraphPad Software, Inc. USA) after arcsin transformation of percentage values. Differences between mean percentages were analyzed by one-way ANOVA. A value of $P < 0.05$ was considered to be statistically significant

1.8 *In vitro* embryo culture

A vital aspect of the experiment was to investigate if MSOT scanning hampers the viability of the oocytes. In order to assess the effect, the sample was rushed back to the lab within 2 hours of MSOT scanning, a constant temperature of 39°c maintained to allow further culture. Post-MSOT imaging BCB infused follicles with a diameter of 3-8mm were aspirated using a vacuum suction machine 18-gauge needle. A group of unscanned ovaries maintained at 39 °c was also infused with BCB at similar concentration formed the control group. Aspiration medium consisted of HEPES-buffered TCM 199 (M 2520) with 26 mM NaHCO3 (S 5761), 1 mM L-glutamine (G 8540), 0. 5-mg/ml polyvinyl alcohol (P 8136), 50 µg/ml gentamicin (G 1264) and 20 U/ml heparin (H 3149). Oocytes (COCs) were retrieved in the same medium without heparin using a stereomicroscope. A total of 130 BCB+ve and 120 BCB-ve oocytes were isolated from the MSOT scanned ovarian follicle (fig) .From the control group oocyte 134 BCB +ve and126 BCB –ve oocytes were aspirated. Oocytes were cultured at 39°C under 5% CO2 in the air and maximum humidity for 46

h. The maturation medium consisted of TCM 199 (M 2154) with 1 mM L-glutamine, 1 mM sodium pyruvate (P 3662), 0.1 mM 2-mercaptoethanol (M 7522), 50 ng/ml epidermal growth factor (E 4127), 50 µg/ml gentamicin and 0.1% (w/v) BSA (A 3311). During the first 24 h of IVM, the medium was supplemented with 10 IU/ ml PMSG and 5 IU/ ml hCG (MSD Tiergesundheit, Germany) and 5 µl/ml ITS (recombinant human insulin, human transferrin, and sodium selenite, I 3146). After 46 h of IVM nuclear maturation rate and developmental potential after parthenogenetic activation and IVF was examined. Also, the DNA damage was assessed by TUNEL assay and relative m RNA expression of a group of apoptotic related Genes were also seen. BCB positive oocytes were selected for further culture and a control group of mixed oocytes were kept. After IVM culture, cumulus investments were removed from the oocytes by gentle pipetting. Oocytes were then fixed for 30 minutes in 0.5% glutaraldehyde (500µl PBS+10 µl 25% glutaraldehyde G-5882), washed in 500 µl PBS for 5 minutes then transferred to 500 µl Hoechst (B2261) stain solution (0.1%). The nuclear status was evaluated by epifluorescence microscopy (UV filter and Carl Zeiss) using standard measures like germinal vesicle breakdown, condensation of chromatin and appearance of the first polar body as confirmation of nuclear maturation

1. 9 Parthenogenetic activation of porcine oocytes

Oocytes were activated chemically to assess their developmental competence. After 46 h IVM culture, COCs were manually denuded by mouth pipetting, then activated by incubating in IVM medium containing 5 µM Ca-ionophore A23187 (C7522) for 5 min at 39ºC under 5% CO2 in air. Oocytes were washed three times in IVM culture medium and incubated in 500 µl droplets containing 2 mM6-DMAP (6-dimethylaminopurine, D2629) and covered with mineral oil in an incubator at 39ºC under 5% CO2 in air for 4 h. After activation, oocytes were cultured in 500 µl porcine zygote medium (PZM 5 IFP) in 4 well dishes (Nunc GmbH, Co.KG, Germany) overlaid

with 500 µl mineral oil (M8410). The dish was incubated undisturbed at 39ºC in 5% CO2 in air for 7 days. Embryo development was observed microscopically and cleavage assessed at 48 h post-activation.

[1] H. Zheng, X.-L. Chen, C.-Q. Zhu, D.-H. Li, Q.-Y. Chen, J.-G. Xu, *Microchem. J.* **2000**, *64*, 263.

[2] A. Rosenthal, D. Razansky, V. Ntziachristos, *IEEE Trans. Med. Imaging* **2010**, *29*, 1275.

[3] X. L. Dean-Ben, V. Ntziachristos, D. Razansky, *IEEE Trans. Med. Imaging* **2012**, *31*, 1154.

[4] D. Razansky, A. Buehler, V. Ntziachristos, *Nat. Protoc.* **2011**, *6*, 1121.

[5] J. Prakash, S. Mandal, D. Razansky, V. Ntziachristos, *IEEE Trans. Biomed. Eng.* **2019**, 1.

[6] L. Ding, X. Luís Deán-Ben, C. Lutzweiler, D. Razansky, V. Ntziachristos, *Phys. Med. Biol.* **2015**, *60*, 6733.

[7] X. Luís Deán-Ben, N. C. Deliolanis, V. Ntziachristos, D. Razansky, *Opt. Lasers Eng.* **2014**, *58*, 119.

Data Tables

Supplementary Table. 1

Genes	Primer Sequences	Annealing Temperature	Product Size (bp)	Accession no.
β- Actin	F-5'GTGGACATCAGGAAGGACCTCTA 3' R-5'ATGATCTTGATCTTCATGGTGCT 3'	58^{0}C	135	U07786
Bak	F-5'CAGCACCATGGGGCAGGTAG3' R-5'AGGCTGGAGGCGATCTTGGT3'	58^{0}C	150	AJ001204.1
Caspase 3	F-5'GCCGAGGCACAGAATTGGAC 3' R-5'GCGCTGCACAAAGTGACTGG3'	58^{0}C	180	AB029345.1
TP53	F-5'CTTTGAGGTGCGTGTTTGTG3' R-5'CGGATCTGGAGGGTGAAATA3'	60^{0}C	152	AF098067.1
Bcl xl	F- 5' TGAAGCAAGCGCTGAGG 3' R- 5' TCACCCCATCCCGGAAG 3'	58^{0}C	117	AF216205.1

Supplementary figures

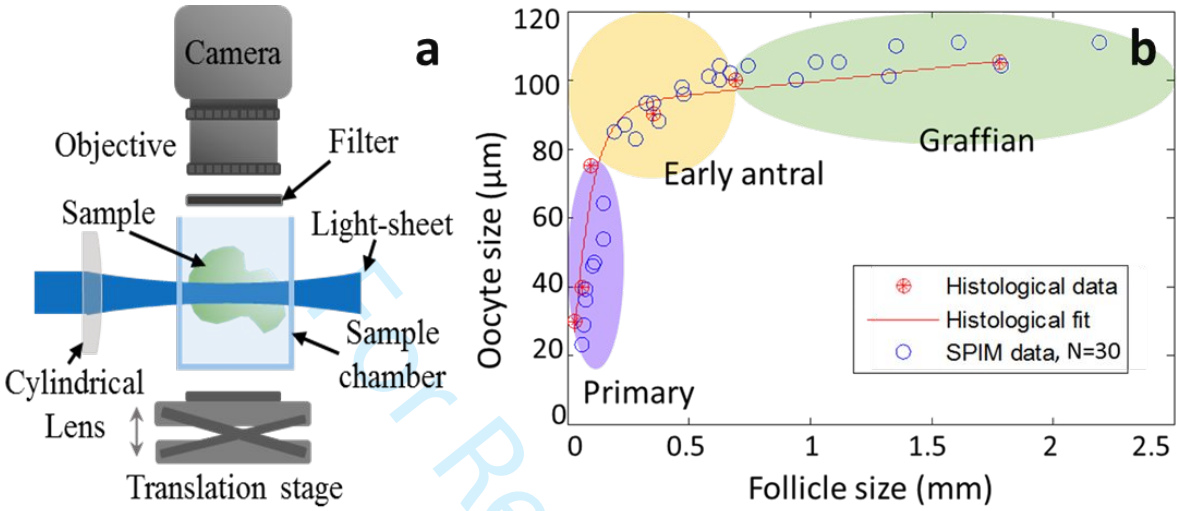

Supplementary Figure 1. Validation of imaging studies with SPIM: (a) The construction and components of the customized SPIM system for ovarian imaging; (b) quantitative analysis of the oocyte size versus the follicle size. Blue circles are data points taken from the SPIM images. 30 data points were taken from SPIM results of two different samples. Histological data of porcine ovarian follicles previously reported in literature are shown in red. R2 (adjusted coefficient of determination) = 0.76, indicating good agreement. Follicles can be categorized according to physical dimensions as: primary (violet) with COC ~60μm, early antral (yellow), with COC ~80μm, or Graafian follicles (green) with COC ~120μm.

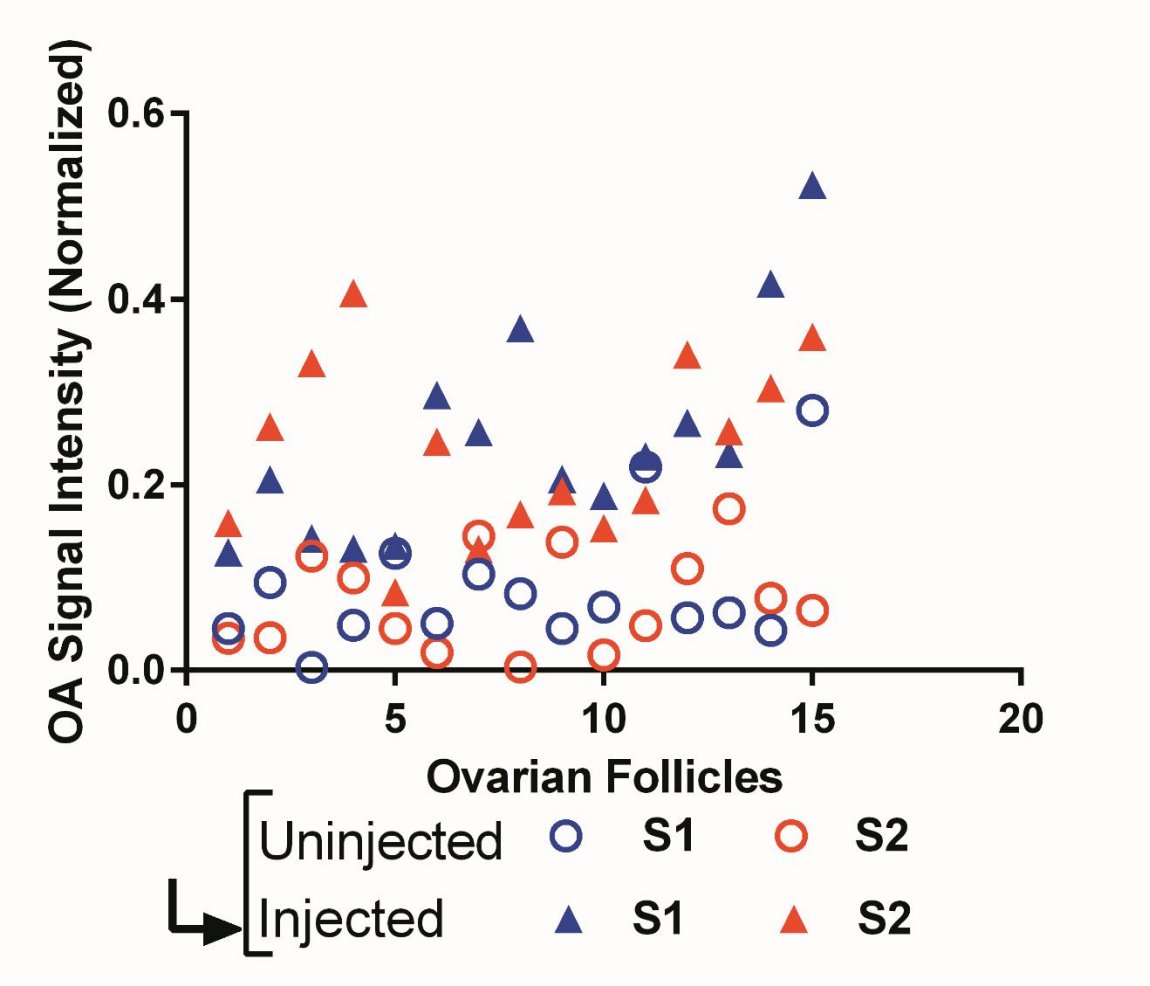

Supplementary Figure 2. Scatter plot of the data-points before (hollow circles) and after injection (solid triangles) for each of the follicles in ovarian sample 1 (blue) and sample 2 (red) is shown. Most of the selected follicles shows increase in signal intensities, however in few there is no observable change (Red – 5, 7; blue – 5, 11), signifying such follicles to be in developing phase, and leading to loss of BCB contrast.

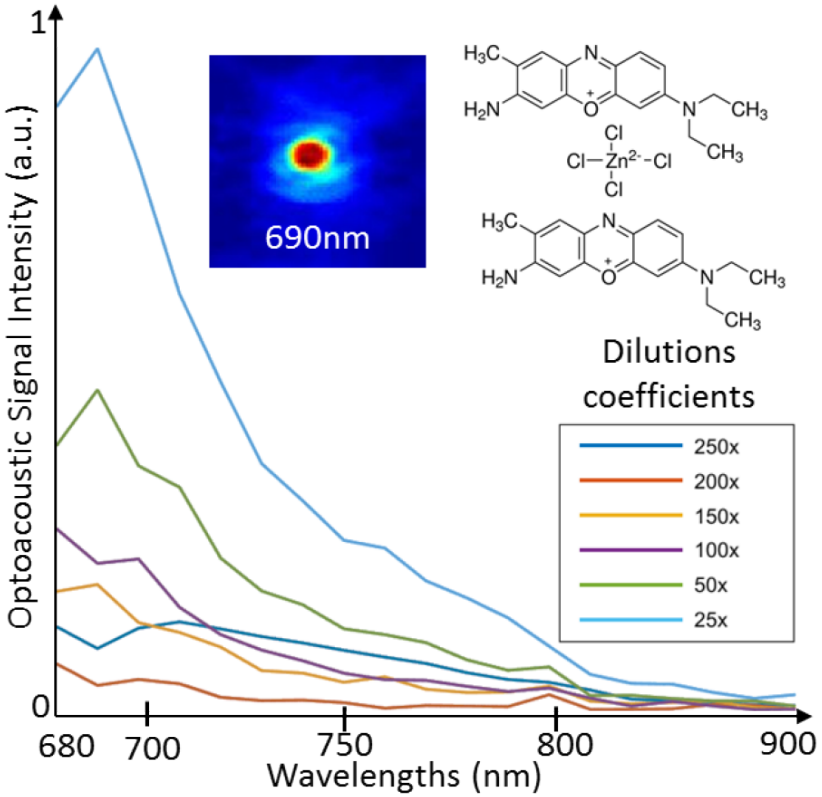

Figure 1. Wavelength dependent optoacoustic signal extinction curve for BCB: The optoacoustic signal responses are measured at several pre-injection dilution coefficients (x =13mM stock solution of BCB/DPBS) using the MSOT (cross-sectional) imaging at varying wavelengths. The BCB solution was perfused through a transparent fine bore polyurethane tubing (0.86mm ID and 1.27mm OD) embedded inside a scattering agar block (7% intralipid by volume). The signal values were determined by fitting an ROI and computing the mean image intensity across the ROI, each for corresponding wavelengths (20WLs were recorded) and dilution coefficients. A representative reconstructed an image (WL 690) is shown in an insert.

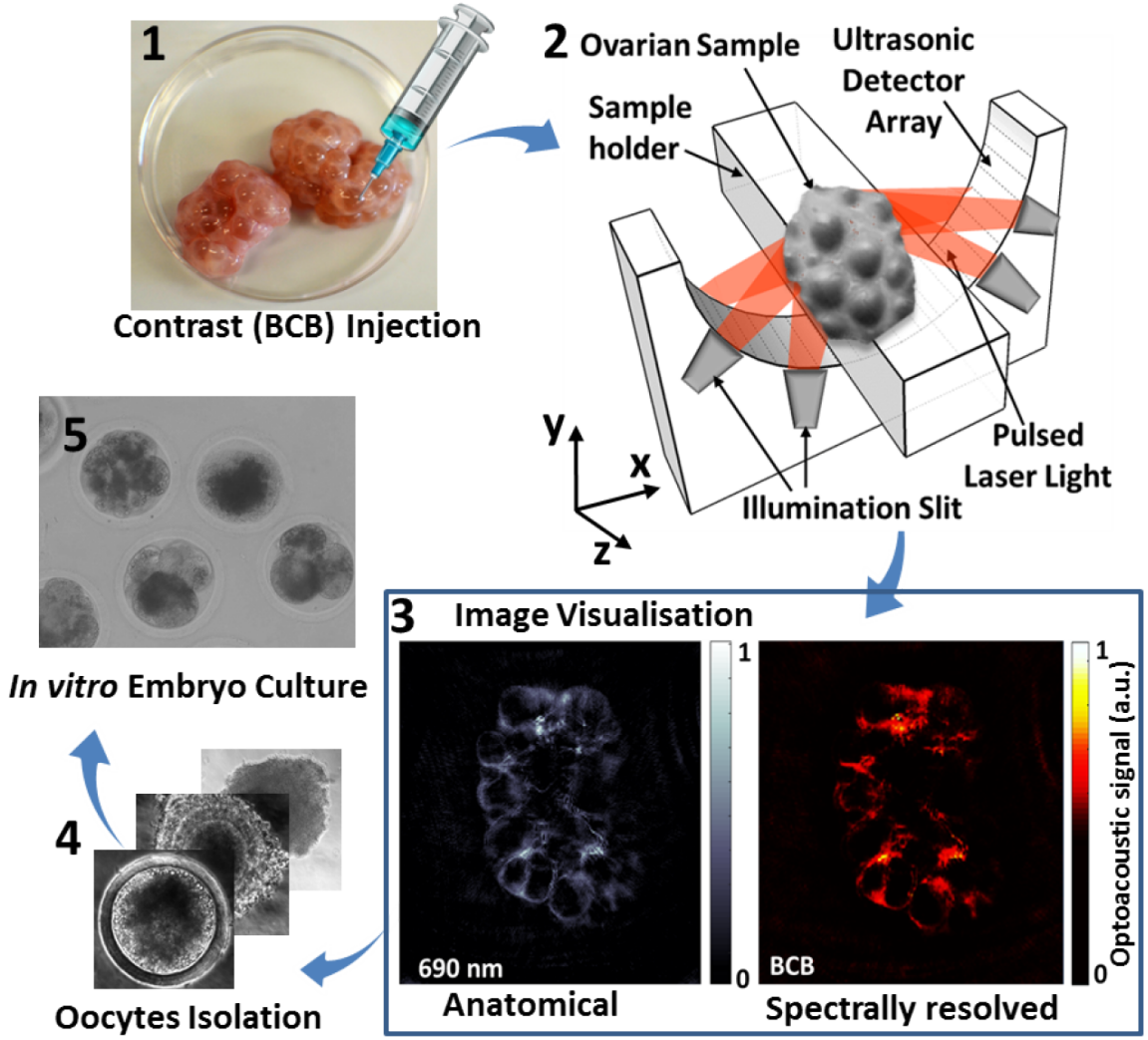

Figure 2. Protocol for ovarian imaging: (1) BCB was injected into the ovarian follicles using a ultrafine needle. (2) After BCB injection ovaries were imaged using MSOT. (3) Single wavelength (690 nm) image of BCB contrast enhanced ovarian follicles are shown in anatomical reference image, and the contrast from BCB molecules is spectrally resolved through a blind unmixing process using 5 wavelengths (4) Following MSOT imaging oocytes were isolated by aspiration and kept for further in vitro culture and analysis. (5) The final stage shows successful formation of the embryo from the isolated oocytes extracted from the BCB+ MSOT scanned ovarian follicles.

a

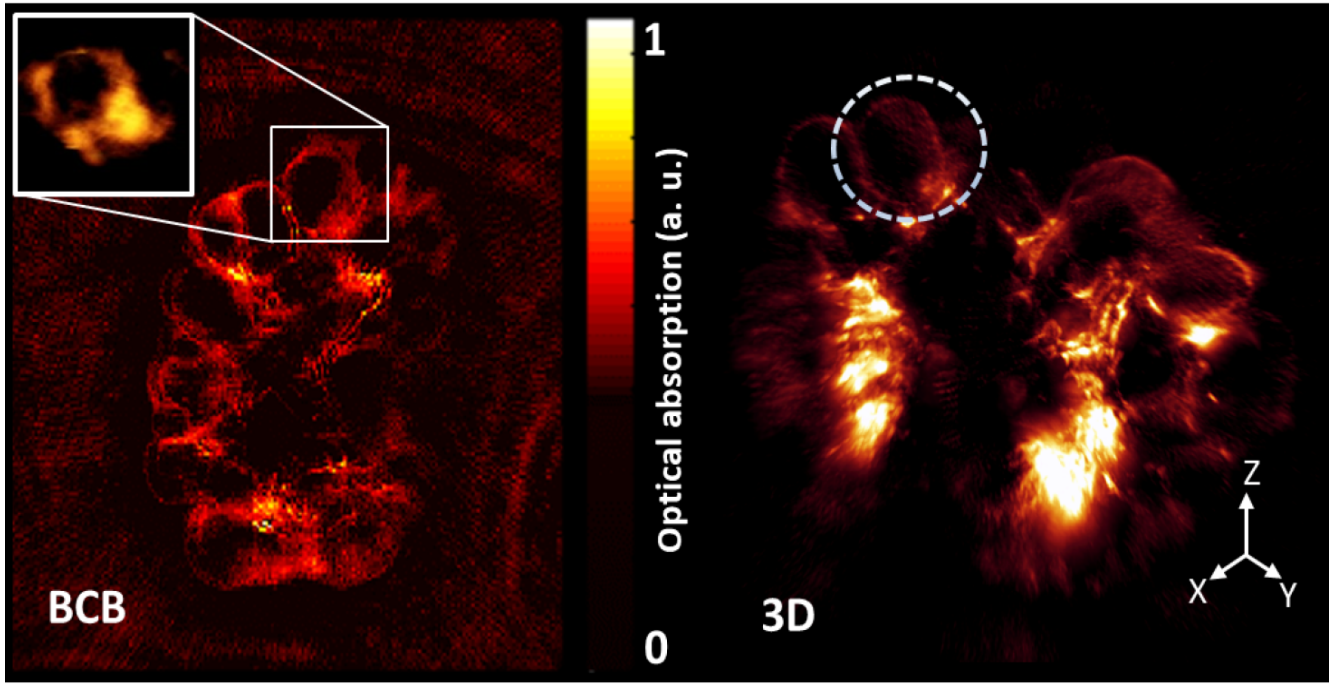

Figure 3. The unmixed BCB channel obtained by using 5 wavelengths(a), the insert shows the original position of the isolated oocyte, and a zoomed in 3D volume rendered version of the selected single oocyte. (b) 3D rendering of entire ovary obtained using z-slacking and fast scanning protocols (~ 5 min/ ovarian sample @ 10 Hz laser pulsation), approximate position of a single viable oocyte is marked.

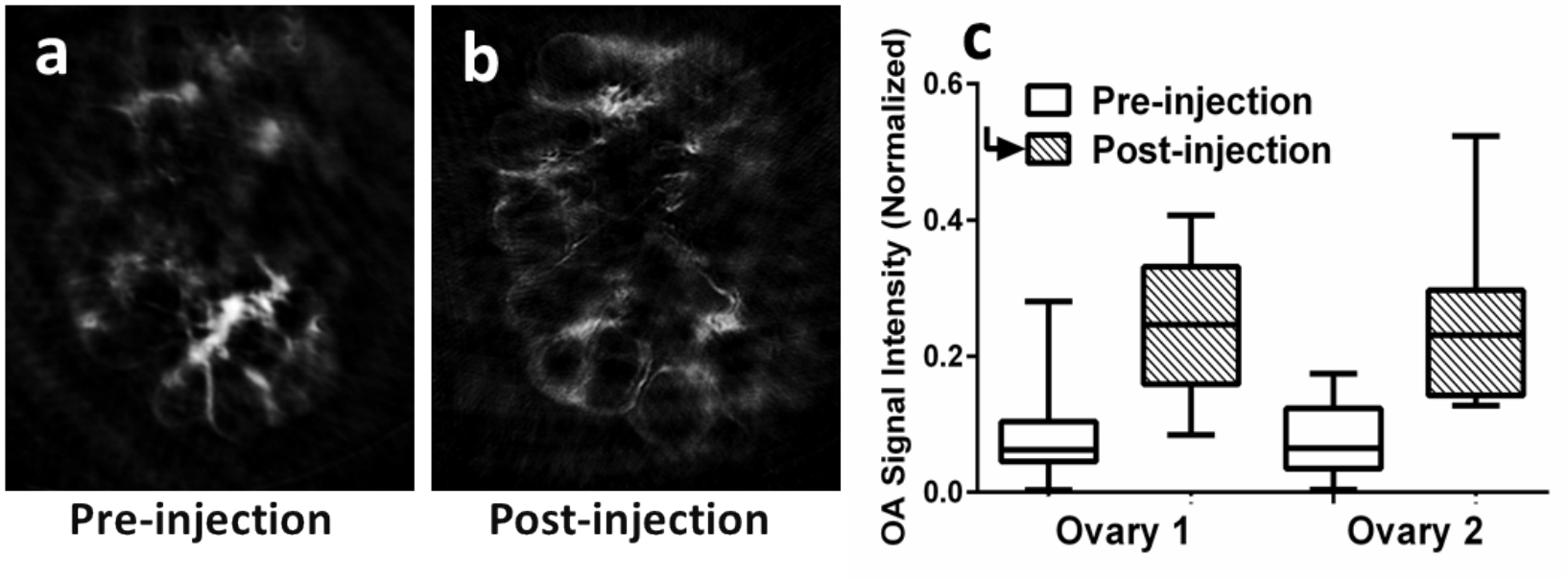

Figure 3. Scan of (intact) ovaries *ex-vivo* before (a) and after (b) injection of BCB (100x diluted 13Mm stock solution) is shown. The post-injection images (normalized) of the ovaries show an increase in relative contrast values. The box-plots of contrast values for two ovaries, before and after the injection are shown (c). Fifteen (15) data-points in each ovary was chosen for evaluation. Supplementary figure 2 shows the scatter plot of the data-points (both before and after injection) for each of the follicles in individual ovaries.

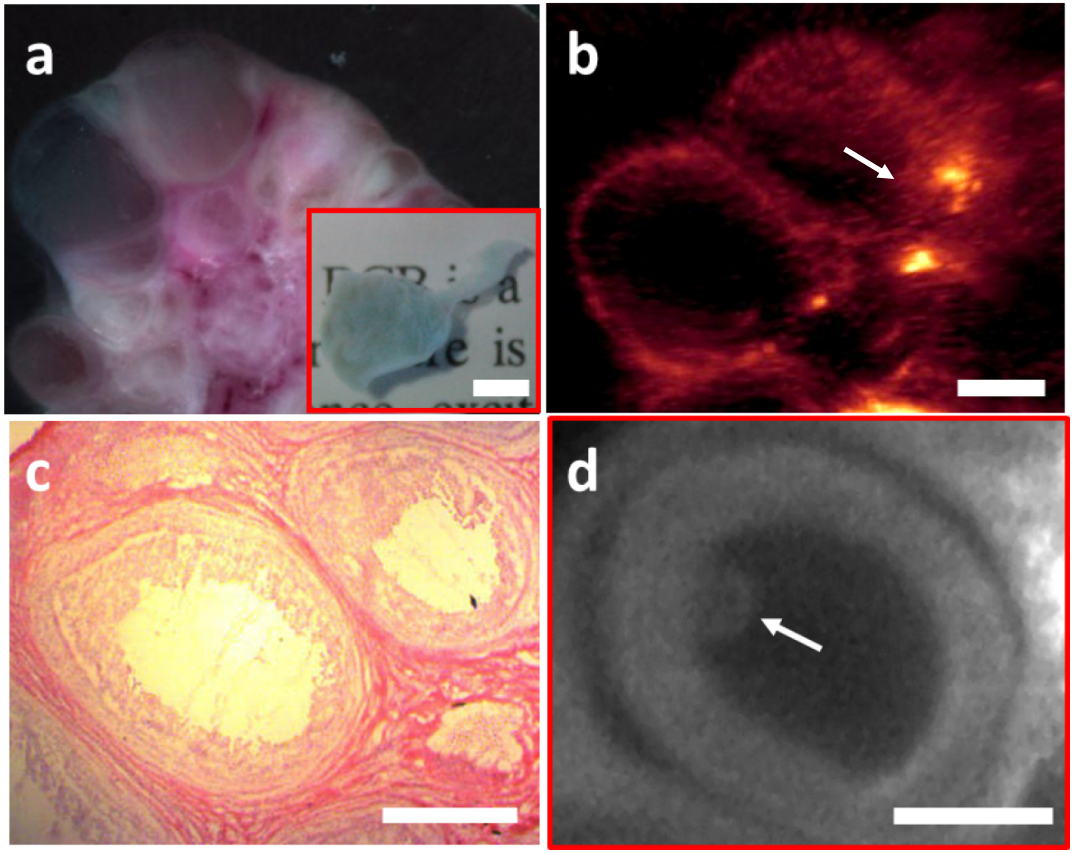

Figure 4. The cryosliced image of BCB+ porcine ovary (a), and the optoacoustic image of the selected ovarian section is shown (b). The histological evaluation was done using H&E stains (c), and validated using the SPIM imaging (d). Insert in (a) shows an isolated follicle which was cleared and imaged using SPIM to obtain the corresponding anatomy for validation (d), the arrow points to the attached COC. [Scalebars ≈1 mm]

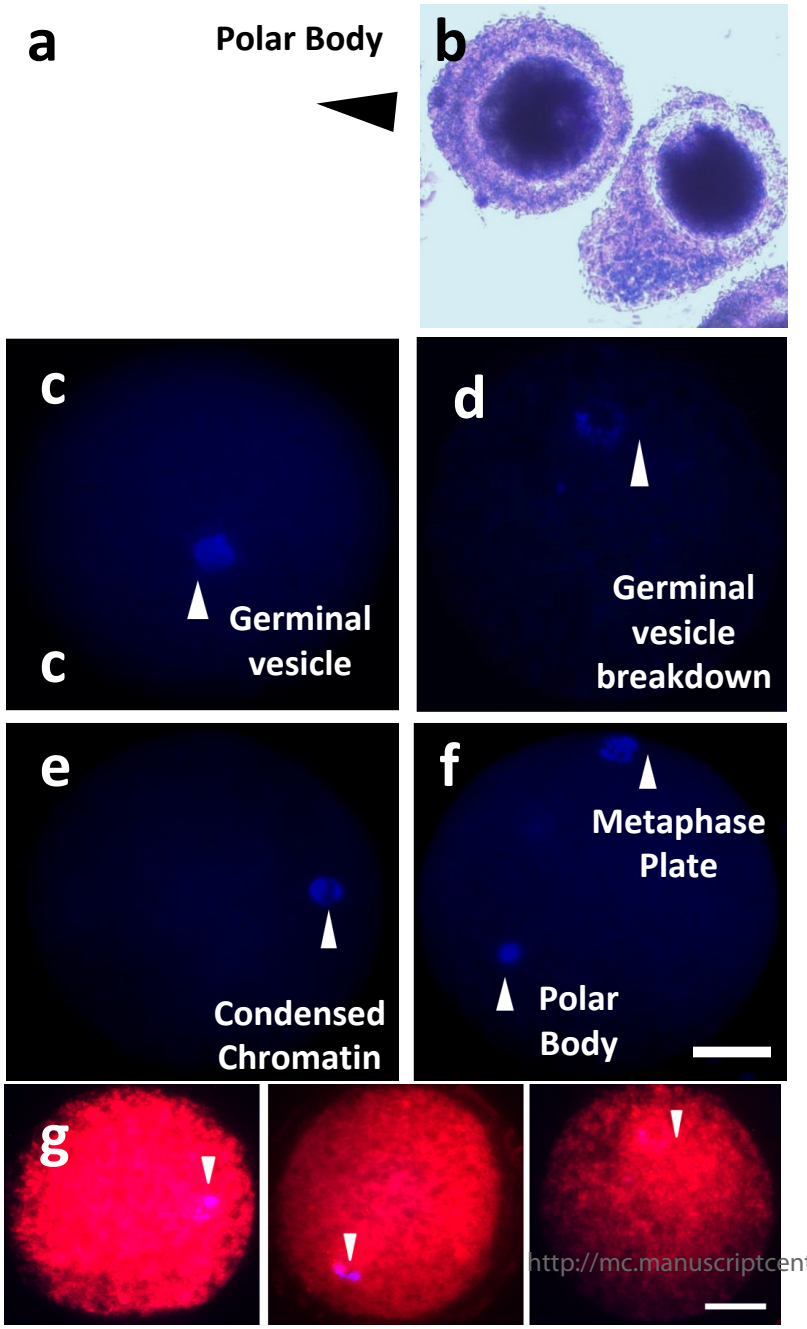

Figure 5. Progression of BCB stained oocytes through different stages of maturation: (a) immature oocyte (b) Germinal Vesicle breakdown stage (c) appearance of first polar body and (d) Mature oocyte with visible polar body and metaphase plate. Mitochondrial distribution of (e) BCB+ ve oocytes showing uniform distribution with polar body and metaphase plate, (f) a control oocyte showing uniform distribution with polar body and metaphase plate and (g) BCB –ve oocyte arrested at germinal vesicle breakdown stage with non uniform mitochondrial distribution. The cumulative IVF Fertilization rate post treatment and MSOT scanning achieved is 76%(39/51) All scale bars indicate 100 µm.

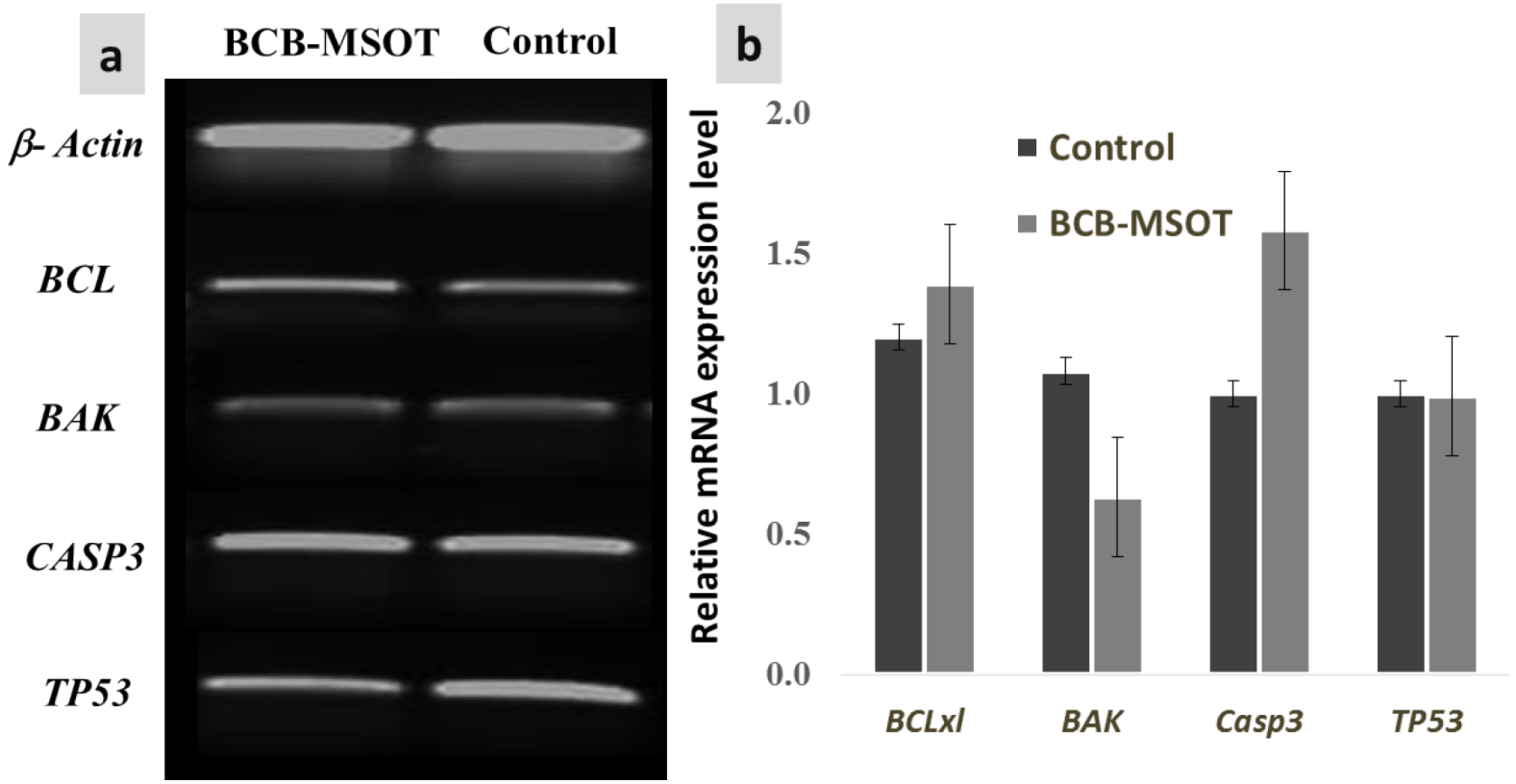

Figure 6. The Reverse transcription PCR of (a) apoptosis associated and stress associated genes in MSOT scanned oocytes (exposure 5-20 mins). The panel (b) shows the statistical significances for tests conducted with ß-Actin, BCL BAK and TP53 -- no significant DNA damage due to BCB and/or MSOT scanning is observed.

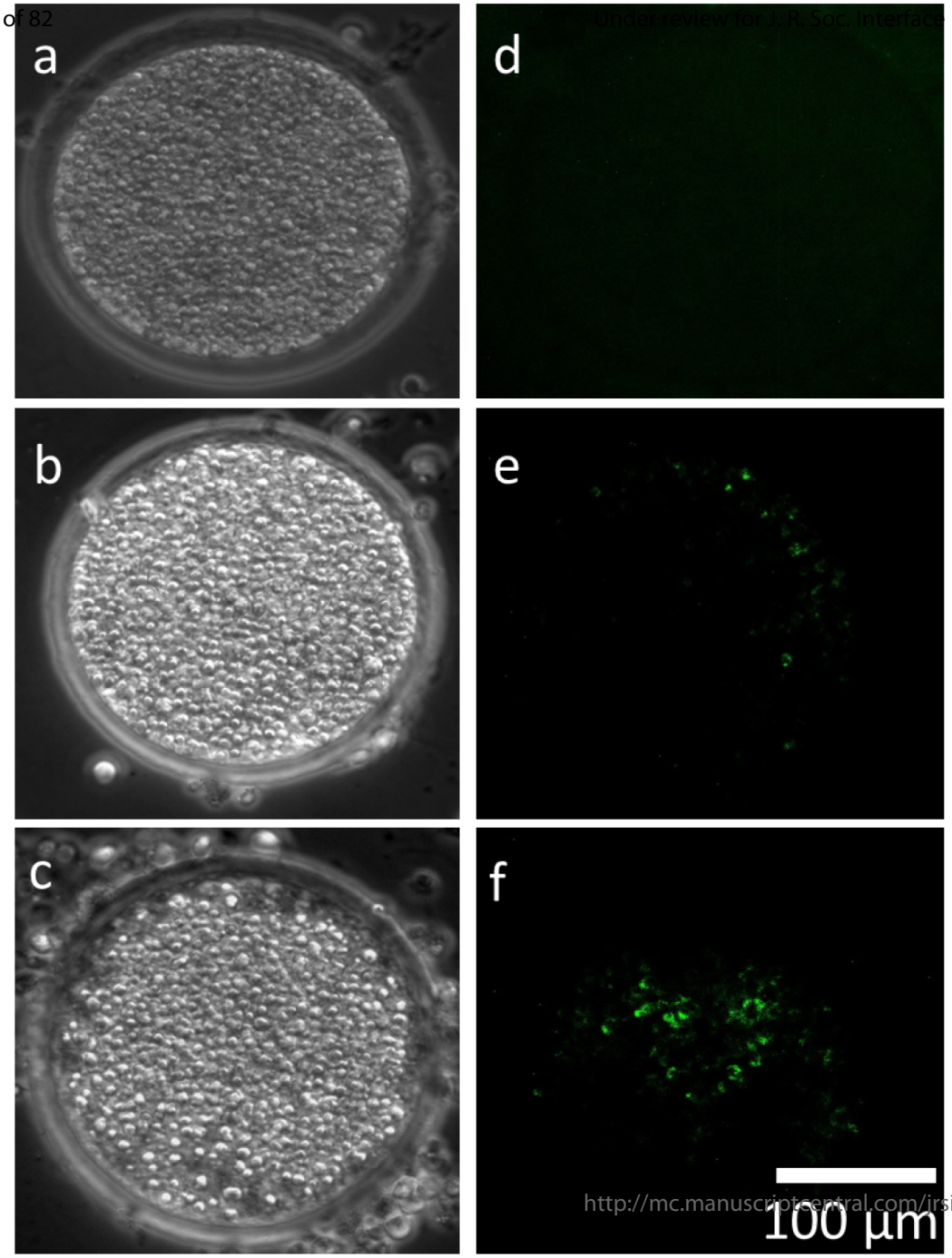

Figure 7. DNA fragmentation detection (bright-field images) by TUNEL assay (a) Porcine oocyte with no detectable DNA fragmentation, (b) BCB +ve porcine oocyte with DNA fragmentation, and (c) control oocyte with DNA fragmentation. The corresponding fluorescent channel images of (a-c) are shown (d-f) on the same scale.

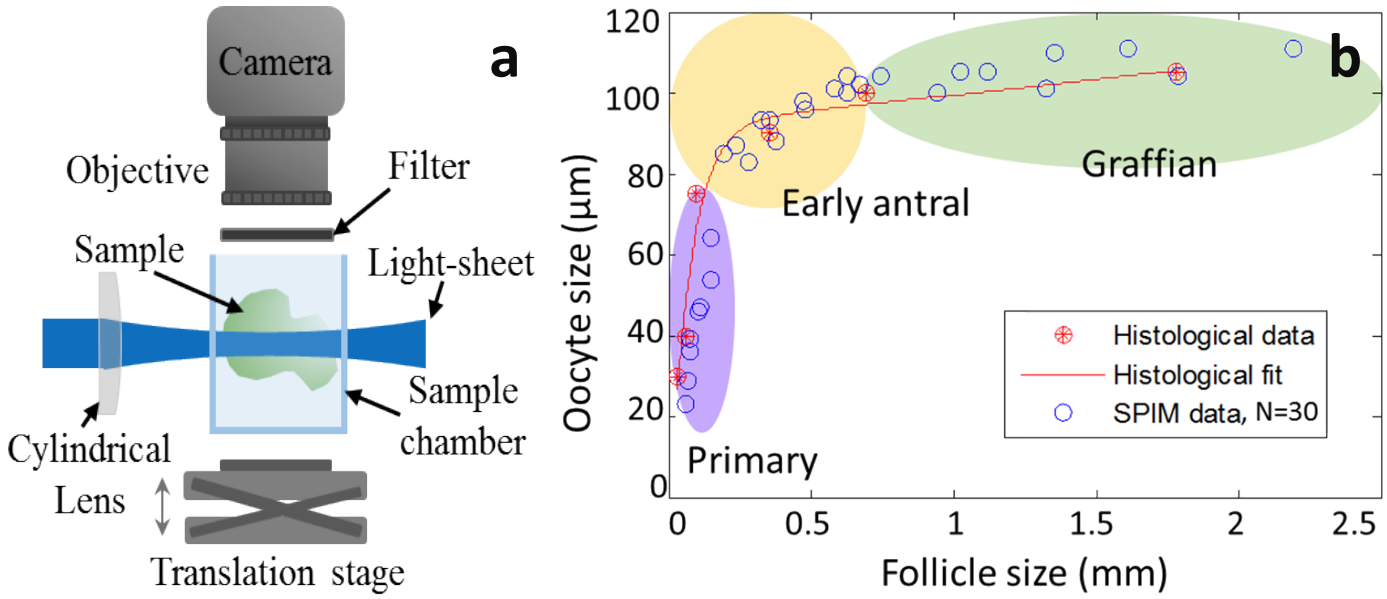

Supplementary Figure 1. Validation of imaging studies with SPIM: (a) The construction and components of the customized SPIM system for ovarian imaging; (b) quantitative analysis of the oocyte size versus the follicle size. Blue circles are data points taken from the SPIM images. 30 data points were taken from SPIM results of two different samples. Histological data of porcine ovarian follicles previously reported in literature are shown in red. R2 (adjusted coefficient of determination) = 0.76, indicating good agreement. Follicles can be categorized according to physical dimensions as: primary (violet) with COC ~60μm, early antral (yellow), with COC ~80μm, or Graafian follicles (green) with COC ~120μm.

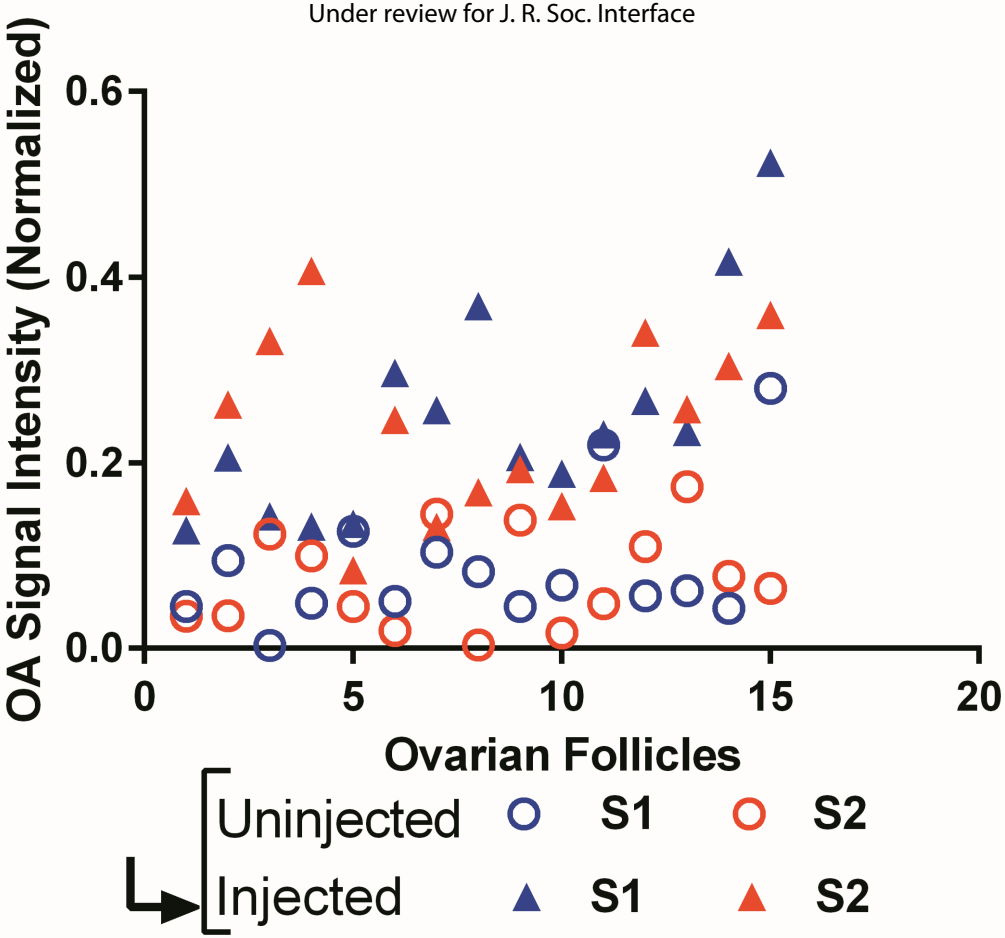

Supplementary Figure 2. Scatter plot of the data-points before (hollow circles) and after injection (solid triangles) for each of the follicles in ovarian sample 1 (blue) and sample 2 (red) is shown. Most of the selected follicles shows increase in signal intensities, however in few there is no observable change (Red – 5, 7; blue – 5, 11), signifying such follicles to be in developing phase, leading to loss of BCB contrast.